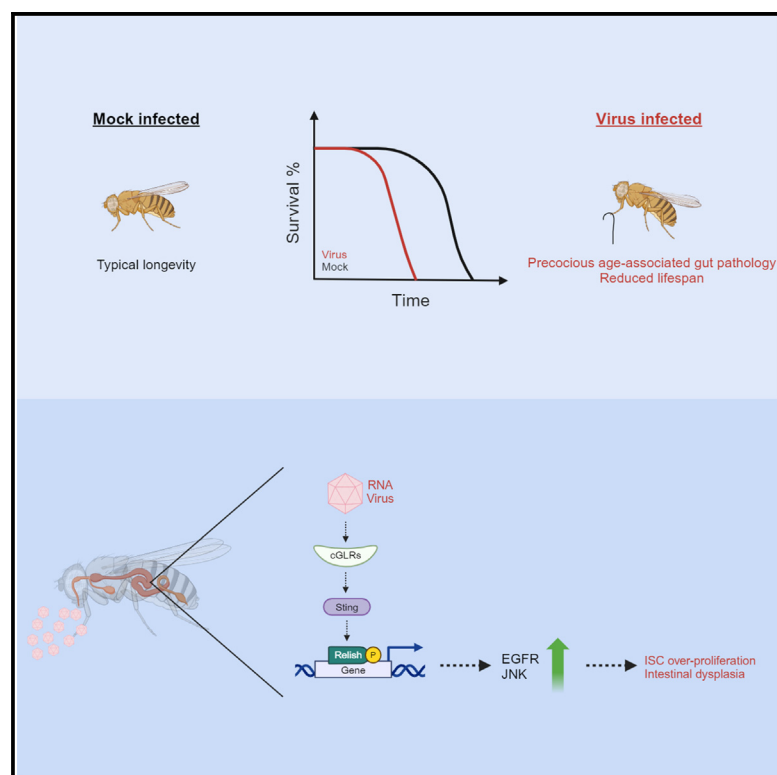# Viral infection disrupts intestinal homeostasis via Sting-dependent NF-κB signaling in *Drosophila*

Graphical abstract

Authors

Jared C. Nigg,
Mauro Castelló-Sanjuán,
Hervé Blanc, ..., Xavier Godron,
Allison J. Bardin, Maria-Carla Saleh

Correspondence

carla.saleh@pasteur.fr

In brief

Nigg et al. show that enteric viral infection accelerates the onset of age-associated gut pathology in *Drosophila* by inducing sustained over-proliferation of intestinal stem cells via chronic NF-κB signaling. These findings reveal a novel role for Sting-dependent NF-κB signaling in regulating epithelial turnover.

Highlights

- Viral infection induces sustained over-proliferation of intestinal stem cells

- Chronic NF-κB signaling accelerates the onset of age-associated gut pathology

- Viral infection modulates epithelial turnover by novel mechanisms

- Sting-dependent NF-κB signaling regulates intestinal stem cell activity

Article

Viral infection disrupts intestinal homeostasis via Sting-dependent NF-κB signaling in *Drosophila*

Jared C. Nigg,[1] Mauro Castelló-Sanjuán,[1] Hervé Blanc,[1] Lionel Frangeul,[1] Vanesa Mongelli,[1] Xavier Godron,[2] Allison J. Bardin,[3] and Maria-Carla Saleh[1,4,5,*]

[1]Institut Pasteur, Université Paris Cité, CNRS UMR3569, Viruses and RNA Interference Unit, 75015 Paris, France
[2]DNA Script SAS, 67 Avenue de Fontainebleau, 94270 Le Kremlin-Bicêtre, France
[3]Institut Curie, Université PSL, Sorbonne Université, CNRS UMR3215, INSERM U934, Genetics and Developmental Biology, 75005 Paris, France
[4]X (formerly Twitter): @SalehLabParis
[5]Lead contact
*Correspondence: carla.saleh@pasteur.fr
https://doi.org/10.1016/j.cub.2024.05.009

SUMMARY

Host-microbe interactions influence intestinal stem cell (ISC) activity to modulate epithelial turnover and composition. Here, we investigated the functional impacts of viral infection on intestinal homeostasis and the mechanisms by which viral infection alters ISC activity. We report that Drosophila A virus (DAV) infection disrupts intestinal homeostasis in *Drosophila* by inducing sustained ISC proliferation, resulting in intestinal dysplasia, loss of gut barrier function, and reduced lifespan. We found that additional viruses common in laboratory-reared *Drosophila* also promote ISC proliferation. The mechanism of DAV-induced ISC proliferation involves progenitor-autonomous epidermal growth factor receptor (EGFR) signaling, c-Jun N-terminal kinase (JNK) activity in enterocytes, and requires Sting-dependent nuclear factor κB (NF-κB) (Relish) activity. We further demonstrate that activating Sting-Relish signaling is sufficient to induce ISC proliferation, promote intestinal dysplasia, and reduce lifespan in the absence of infection. Our results reveal that viral infection can significantly disrupt intestinal physiology, highlight a novel role for Sting-Relish signaling, and support a role for viral infection in aging.

INTRODUCTION

To maintain homeostasis in the face of microbial and environmental assaults, the intestinal epithelium undergoes continuous cellular turnover driven by the proliferation of intestinal stem cells (ISCs) to replace old or damaged differentiated cells.[1,2] Immune and stress signaling pathways integrate environmental cues including injury, infection, and nutrient status to modulate ISC proliferation rates, differentiated cell death, and the balance of differentiation programs in proliferating ISCs.[3] Although these processes are essential, they must be tightly regulated to ensure intestinal function and integrity.[4] Intestinal homeostatic defects are underlying drivers of numerous conditions in mammals including inflammatory bowel disease,[5] colorectal cancer,[6] and loss of gut barrier function.[7] Consequently, maintenance of intestinal homeostasis is a primary determinant of lifespan and healthspan.[8–10] Understanding how host-microbe interactions modulate intestinal homeostatic processes is thus crucial for developing interventions to mitigate deleterious impacts of infection and promote healthy aging.

Drosophila melanogaster is a tractable model at the forefront of efforts investigating how host-microbe interactions impact intestinal homeostasis. The regulatory mechanisms directing ISC proliferation in the mammalian intestine and the *D. melanogaster* midgut are highly similar,[1] both involving conserved signaling pathways, including the c-Jun N-terminal kinase (JNK), the Janus

kinase-signal transducer and activator of transcription (JAK-STAT), epidermal growth factor receptor (EGFR), Wingless, and Hippo pathways. Importantly, the intestinal epithelia of mammals and *D. melanogaster* are both composed of functionally analogous differentiated cells maintained by ISCs.[11] The *D. melanogaster* intestinal epithelium primarily consists of differentiated absorptive enterocytes (ECs) and secretory enteroendocrine cells (EEs) sustained by ISCs that proliferate and partially differentiate into progenitor cells termed enteroblasts and pre-EEs, which themselves fully differentiate into ECs or EEs, respectively.[12–14]

Studies in *D. melanogaster* have revealed that pathogenic bacterial infection activates JNK signaling in damaged ECs, causing the release of Unpaired (Upd) cytokines that directly and indirectly stimulate cell-autonomous JAK-STAT and EGFR signaling, respectively, in ISCs.[15,16] This triggers a transient burst of ISC proliferation that is required to repair epithelial damage.[15] In contrast, commensal bacteria stimulate low levels of ISC proliferation, promoting basal levels of epithelial renewal.[15] Age-associated shifts in the composition, abundance, and distribution of the commensal microbiota provoke chronic stress signaling that stimulates sustained over-proliferation of ISCs and disrupts homeostatic differentiation programs.[15,17–21] This process promotes intestinal dysplasia and is proposed to drive progressive age-associated gut dysfunction and mortality.[17,22] Indeed, loss of gut barrier function is observed prior to and is
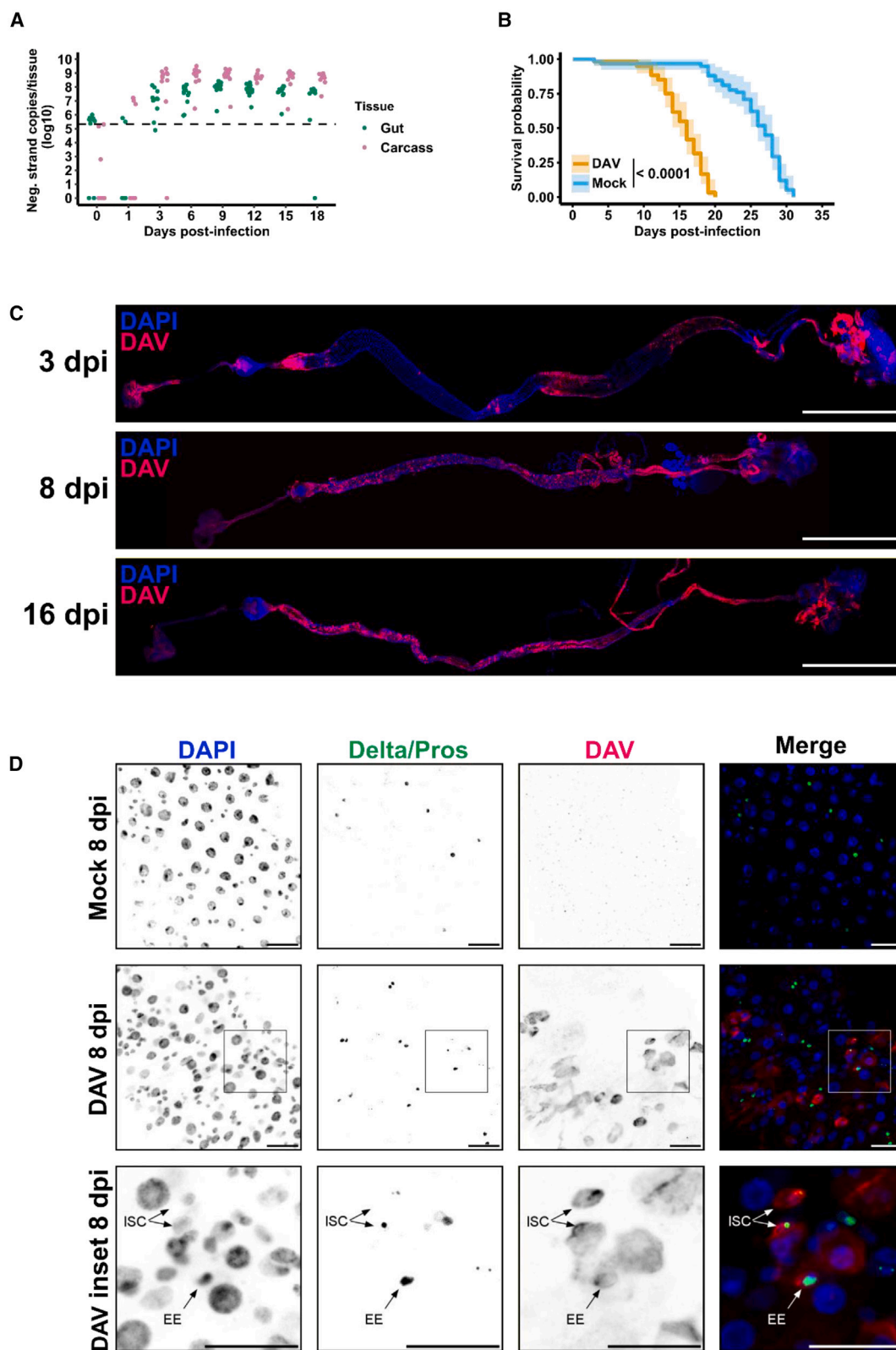
Figure 1. Orally acquired DAV persistently infects the adult midgut

(A) Negative-strand-specific RT-qPCR of DAV RNA in carcasses and dissected midguts from flies orally infected with DAV. The dashed line indicates the limit of detection.

predictive of death.[4,19] However, the precise causal relationships between dysregulated ISC proliferation, loss of gut barrier function, and death are uncertain.

Viral infections can promote intestinal pathology by disrupting intestinal homeostasis in mammals, but the molecular mechanisms underlying virus-driven homeostatic defects have not been explored in detail.[23–26] In this respect, *D. melanogaster* represents an excellent model to mechanistically investigate how host-virus interactions modulate gut epithelial turnover. Viral infections are prevalent in *D. melanogaster* and typically manifest as persistent infections characterized by lifelong viral replication with relatively uncharacterized impacts on host fitness and physiology.[27–29] Prevalent viruses of *D. melanogaster*, including Drosophila C virus (DCV), Nora virus, and Galbut virus, infect the intestinal epithelium,[30–32] but the potential impacts of viral infection on intestinal homeostasis have not been examined.

Drosophila A virus (DAV) is an unclassified, positive-sense single-stranded RNA virus of *D. melanogaster* that is prevalent in field-collected and laboratory-reared flies.[28,29,33] Little is known about DAV, although it is reported that DAV infection reduces lifespan and detection of DAV reads in midgut, RNA sequencing (RNA-seq) data suggest that this virus replicates in intestinal tissues.[34,35] Reanalysis of published RNA-seq data suggested that DAV and other enteric RNA viruses stimulate innate immune responses and epithelial repair pathways in the gut.[28] Because of these findings and our previous observation that orally acquired DAV persistently infects adult flies,[36] we focused on oral DAV infection to elucidate the impact of host-virus interactions on intestinal homeostasis. Here, we demonstrate that DAV infection induces sustained ISC proliferation and accelerates the development of age-associated intestinal pathology, thereby reducing lifespan in infected flies. Other RNA viruses also caused elevated ISC proliferation, altered gut epithelial morphology, and reduced lifespan, suggesting that modulation of intestinal physiology is a common feature of viral infection. We found that classical epithelial repair pathways and novel mechanisms play roles in virus-induced ISC proliferation and disruption of intestinal homeostasis by viral infection. Our results establish the utility of *D. melanogaster* as a model for studying host-virus interactions in the intestine, identify novel regulators of ISC proliferation, and uncover physiological impacts caused by prevalent viruses.

RESULTS

DAV persistently infects the adult midgut
To determine if DAV infects the midgut, we performed negative-strand-specific RT-qPCR using RNA from midguts and carcasses from orally infected flies. This assay quantifies replicating viral RNA by detecting the replicative negative strand of the DAV genome. We detected DAV replication in midguts and carcasses by 3 days post-infection (dpi) (Figure 1A). Orally acquired DAV persistently infected the midgut and carcass, with high levels

of replicative DAV RNA observed in both tissues until at least 18 dpi (Figure 1A). Oral DAV infection was not acutely lethal. Instead, DAV-infected flies exhibited reduced lifespans compared with mock-infected controls at 25°C (Figure S1A) and 29°C (Figure 1B). We performed all subsequent experiments at 29°C to facilitate the comparison of infection phenotypes across all potential fly genotypes, including those encoding temperature-sensitive expression constructs. Female flies were used for all experiments.

To further characterize enteric DAV infection, we determined the regional and temporal tropism of DAV in the gut by RNA fluorescence *in situ* hybridization (FISH). At 3 dpi, we detected DAV RNA in isolated patches throughout the entire alimentary canal (Figures 1C and S2A). DAV RNA was spread throughout the gastrointestinal tract by 8 dpi, a pattern that continued until at least 16 dpi (Figures 1C and S2A). We next determined the cellular tropism of DAV in the midgut by immunofluorescence with antibodies against the DAV capsid, Delta (an ISC marker),[37] and Prospero (Pros; an EE marker).[37] At 8 dpi, we primarily observed infection in large Delta/Pros negative ECs; however, we occasionally observed infection of Delta-positive ISCs and Pros-positive EEs (Figure 1D).

DAV infection reduces lifespan by driving over-proliferation of ISCs
The midgut epithelia in DAV-infected flies exhibited irregularities, characterized by aberrant spatial organization and altered size distribution of nuclei (Figure 1D). This phenotype resembles age-dependent intestinal dysplasia, which is driven by over-proliferation of ISCs and disruption of cellular differentiation programs due to chronic stress signaling triggered by commensal dysbiosis in aged flies.[15,17,18,21] We hypothesized that DAV infection may similarly stimulate chronic mitogenic signaling and premature development of intestinal dysplasia due to sustained ISC over-proliferation. We thus measured ISC proliferation in DAV- and mock-infected flies by immunofluorescence with an antibody against phosphorylated histone H3 (PH3).[13] DAV infection induced ISC over-proliferation by 4 dpi, which continued for the lifetime of infected flies (Figure 2A). Reported age-associated ISC proliferation levels vary between studies and fly genotypes; however, aged w^{1118} flies are generally reported to exhibit 20–50 PH3+ cells/midgut,[18,38,39] a range consistent with our observations in DAV-infected flies from 6 dpi (Figure 2A). DAV-infected germ-free (GF) flies also exhibited premature intestinal dysplasia (Figures 2B and S1B) and DAV-induced ISC proliferation levels were not significantly different between conventionally-reared (CR) and GF flies at 8 dpi (Figure 2B). Moreover, the median survival of DAV-infected flies relative to mock-infected controls was not significantly different between CR or GF conditions (Figures S1C and S2D). DAV infection also induced ISC proliferation at 25°C (Figure S1E). Together these results indicate that DAV infection induces sustained

(B) Survival of mock-infected and DAV-infected flies maintained at 29°C. Shaded regions: 95% confidence intervals. Three biological replicates (*n* = 20 flies/replicate) were analyzed. The *p* value from a log-rank (Mantel-Cox) test is shown.

(C) RNA FISH of positive strand DAV RNA in guts from DAV-infected flies. Scale bars, 1 mm.

(D) Representative images of R4 midgut regions from mock-infected and DAV-infected flies. Boxes in the middle panels indicate the region in the lower panels. Delta+ and Pros+ cells are distinguished by membrane/vesical and nuclear staining, respectively. Arrows indicate DAV-infected ISCs or EEs. Scale bars, 50 μm. See also Figures S1 and S2.
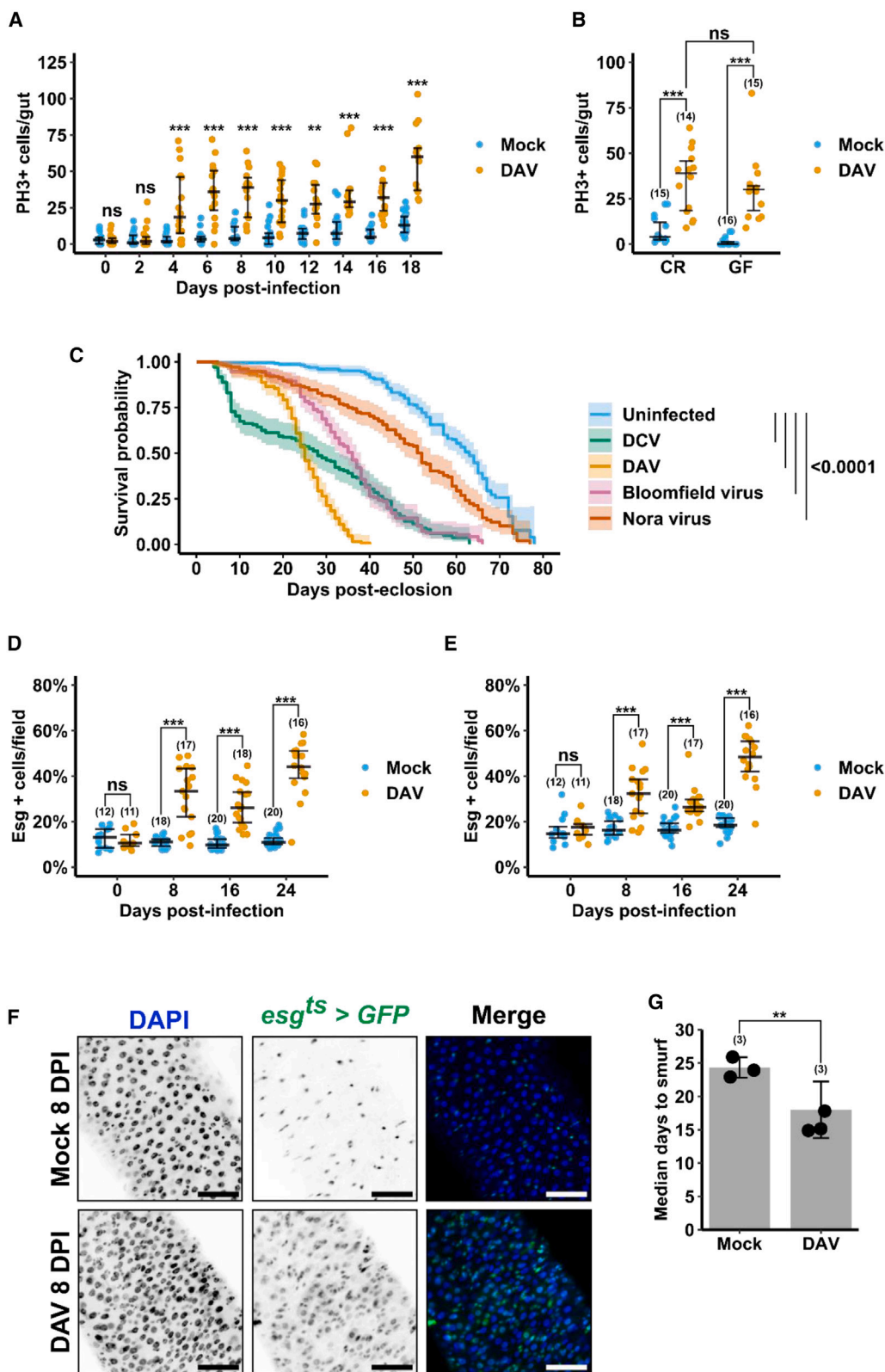
Figure 2. DAV infection disrupts intestinal homeostasis
(A) Quantification of PH3+ cells in midguts from mock-infected or DAV-infected flies.
(B) Quantification of PH3+ cells at 8 dpi in midguts from mock-infected or DAV-infected flies maintained under CR or GF conditions.

(legend continued on next page)

over-proliferation of ISCs, promotes premature intestinal dysplasia, and reduces lifespan independent of the microbiota.

To determine if elevated ISC proliferation is specific to DAV, we measured ISC proliferation at 20 days post-eclosion (dpe) in isogenic wild-type (w^{1118}) flies harboring persistent infections with DAV, DCV, Nora virus, or Bloomfield virus (all RNA viruses known to infect the midgut). Persistent infections with any of the viruses were associated with elevated ISC proliferation, irregular epithelial morphology at 20 dpe, and reduced lifespan (Figures 2C, S1F, and S1G).

A hallmark of age-dependent intestinal dysplasia and loss of intestinal homeostasis is an accumulation of polyploid cells marked by continuous expression of the progenitor cell marker, Escargot (Esg).[17,40] We infected flies expressing GFP under the control of a temperature-sensitive esg-Gal4 driver (esg-Gal4; tub-Gal80 UAS-GFP,[13] referred to as esg^{ts}) to follow the accumulation of Esg+ cells during DAV infection. The proportion of Esg+ cells was significantly higher in DAV-infected midguts compared with mock-infected controls in the R2 and R4 midgut regions at 8, 16, and 24 dpi (Figures 2D–2F).

Loss of gut barrier function accompanying intestinal dysplasia is proposed as a driver of mortality in aged flies, although the causal relationship between barrier decay and death is uncertain.[4,19,41] Given that DAV infection accelerates the development of intestinal dysplasia, we used the "Smurf assay"[4] to measure intestinal barrier function during DAV infection. As expected, mock-infected flies showed age-dependent loss of intestinal barrier function, with an average median time to Smurf of 24.3 dpi (Figure 2G). DAV infection significantly accelerated the onset of intestinal barrier dysfunction, with an average median time to Smurf of 16 dpi (Figure 2G), suggesting that precocious loss of gut barrier function may underlie reduced lifespan in DAV-infected flies. This possibility must be considered with caution because loss of gut barrier function could signal impending death through means indirectly related to barrier integrity.

To directly test a role for DAV-induced ISC proliferation in accelerating loss of intestinal homeostasis and reducing lifespan, we inhibited ISC proliferation by overexpressing the cyclin-dependent kinase inhibitors Wee1 and Dacapo in ISCs.[42] This was accomplished using the ISC-specific, temperature-sensitive esg-Gal4 Su(H)GBE-Gal80 tub-Gal80^{ts} system (referred to as esg^{ts}; Su(H)-Gal80).[43] Overexpression of Wee1 and Dacapo in ISCs significantly reduced ISC proliferation levels compared with control flies (Figure 3A). Strikingly, reducing ISC proliferation significantly prolonged lifespan during DAV infection (Figures 3B and 3C), indicating that DAV-induced ISC proliferation contributes to lifespan reduction. Prolonged lifespan accompanying inhibited ISC proliferation was not due to

reduced DAV replication (Figures 3D and 3E). Our findings suggest that DAV infection reduces lifespan by accelerating the onset of classical age-associated intestinal pathologies.

DAV infection upregulates immune, stress, and epithelial repair pathways in the intestine

We sequenced transcriptomes of mock- and DAV-infected midguts at 6 and 12 dpi to identify signaling pathways that may play roles in DAV-induced ISC proliferation (Data S1). We sequenced midguts from CR and GF flies to distinguish differential expression patterns driven independently by DAV from those requiring microbiota input. Notably, negative-strand DAV RNA levels were similar in midguts from GF and CR flies at both time points (Figure S3A). DAV infection in CR or GF flies induced upregulation of genes belonging to the primary pathways responsible for regulating ISC proliferation, the EGFR and JAK-STAT pathways (Figures 4A and 4B). We noticed a trend toward more significant DAV-induced upregulation of EGFR and JAK-STAT pathway genes in midguts from GF flies compared with midguts from CR flies. We tested the significance of these differences by directly comparing gene expression in midguts from DAV-infected CR flies with midguts from DAV-infected GF flies. Only one EGFR- or JAK-STAT-related gene was differentially expressed between these conditions (Figures 4A and 4B). These results suggest that DAV infection can stimulate EGFR and JAK-STAT signaling in the absence of the microbiota and do not support a major role for the microbiota in modulating EGFR or JAK-STAT pathway activation during DAV infection. Genes encoding the JNK pathway transcription factors Ets21C and Sox21a were also upregulated in DAV-infected midguts (Figures 4A and 4C). Additionally, DAV infection induced modest, time point/condition-dependent upregulation of other JNK-related genes (Figure 4C). Our results suggest that DAV infection may induce classical midgut epithelial repair mechanisms by activating the EGFR, JAK-STAT, and JNK pathways.

We next investigated DAV-induced immune mechanisms in the midgut. The *D. melanogaster* inducible immune response is classically defined by the Toll and immune deficiency (IMD) pathways.[44] Studies have uncovered roles for the IMD pathway in regulating intestinal homeostasis, suggesting that inducible immune responses have roles in regulating epithelial turnover.[45–47] IMD pathway transcriptional targets were among the most upregulated genes in DAV-infected midguts at 12 dpi in CR and GF flies (Figure 4D; Data S2). A subset of these IMD-responsive genes was expressed significantly higher in DAV-infected midguts from CR flies than those from GF flies (Figure S3B), suggesting that microbiota input may have an additive effect on IMD activation during DAV infection. Toll pathway transcriptional targets

---

(C) Survival of uninfected w^{1118} flies or isogenic w^{1118} flies persistently infected with DAV, DCV, Nora virus, or Bloomfield virus maintained at 25°C. Shaded regions: 95% confidence intervals. Nine biological replicates ($n = 20$ flies/replicate) from three independent experiments were analyzed. The p value from log-rank (Mantel-Cox) tests is shown.

(D and E) Quantification of Esg+ cells in R2 (D) and R4 (E) midgut regions from mock-infected or DAV-infected flies.

(F) Representative images of Esg+ cells in R4 midgut regions from mock-infected or DAV-infected flies at 8 dpi. Scale bars, 50 μm.

(G) Median days until observation of the "Smurf" phenotype in mock-infected or DAV-infected flies. Dots indicate medians of three biological replicates ($n = 20$ flies/replicate). Bar height indicates average of replicate medians.

Error bars in (A), (B), (D), and (E) indicate median with 1st and 3rd quartiles. Error bars in (G) indicate SD. Results were compared by two-way ANOVA with Turkey's multiple comparisons tests (A, B, D, and E) or a two-tailed t test (G); ns, non-significant; *$p < 0.05$; **$p < 0.01$; ***$p < 0.001$. Comparisons in (A) are between mock and DAV for each dpi. Numbers of biological replicates indicated in parentheses.

See also Figure S1.
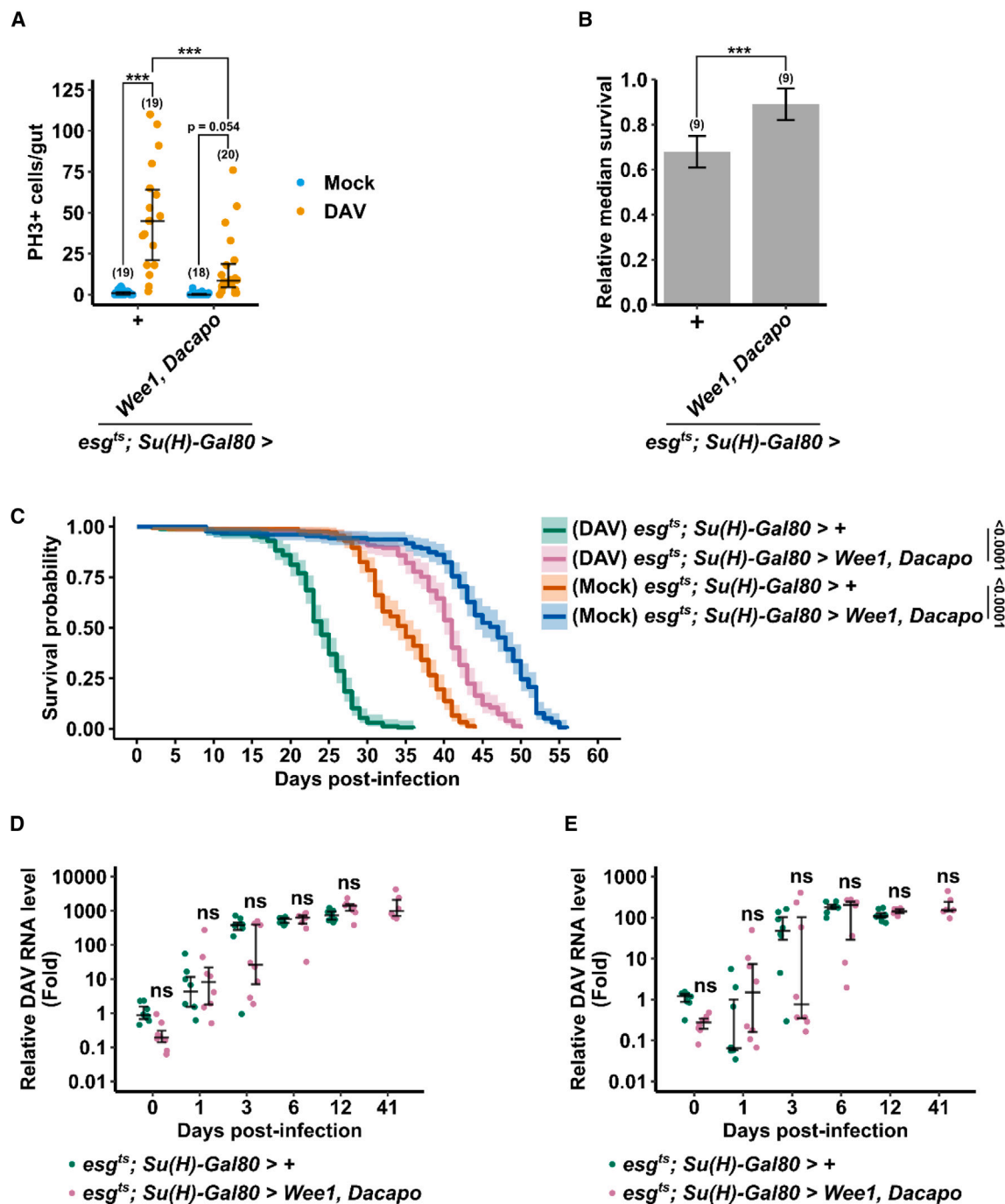
Figure 3. DAV infection reduces lifespan by driving over-proliferation of ISCs

(A) Quantification of PH3+ cells at 8 dpi in midguts from mock-infected or DAV-infected flies of the indicated genotypes.

(B) Relative median survival of DAV-infected flies of the indicated genotypes. Bar height indicates the average of nine biological replicates ($n = 20$ flies/replicate) from three independent experiments.

(C) Survival of mock-infected and DAV-infected flies of the indicated genotypes. Shaded regions: 95% confidence intervals. Nine biological replicates ($n = 20$ flies/replicate) from three independent experiments were analyzed. The p values from log-rank (Mantel-Cox) tests are shown.

(D and E) Relative DAV RNA levels in carcasses or dissected midguts from DAV-infected flies of the indicated genotypes. DAV RNA levels are shown relative to the $esg^{ts}; Su(H)-Gal80 > + 0$ dpi samples. $n = 12$ samples/day for 0–12 dpi. $n = 6$ samples for 41 dpi. Data at 41 dpi were not available for DAV-infected flies with the genotype $esg^{ts}; Su(H)-Gal80 > +$ because they had 100% mortality by 32 dpi.

Error bars in (A), (D), and (E) indicate median with 1st and 3rd quartiles. Error bars in (B) indicate SD. Results were compared by two-way ANOVA with Turkey's multiple comparisons tests (A, D, and E) or two-tailed t test (B); ns, non-significant; ***$p < 0.001$. In (D) and (E), comparisons are between mock and DAV for each dpi.
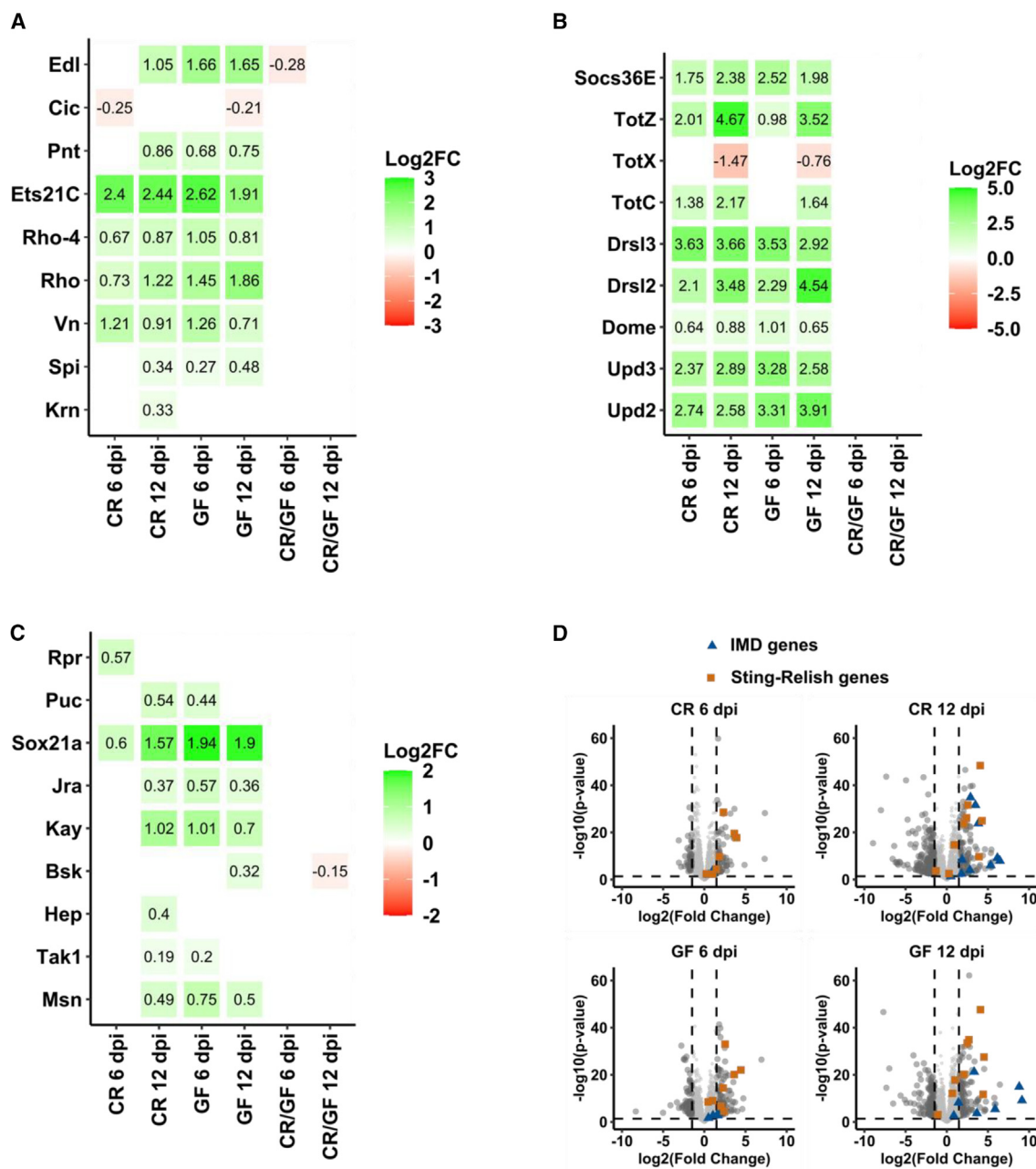
Figure 4. DAV infection upregulates immune, stress, and epithelial repair pathways in the intestine

(A–C) Expression of select genes of the EGFR (A), JAK-STAT (B), or JNK (C) pathways. Text and color indicate the $\log_2$ fold change (Log2FC) of expression in DAV-infected midguts/mock-infected midguts and in DAV-infected CR/GF midguts. Only genes with adjusted p value < 0.05 are shown.

(D) Expression of all genes. Select genes regulated by IMD-Relish or Sting-Relish signaling are highlighted (see Data S2). Expression in DAV-infected midguts/mock-infected midguts is shown. Horizontal dashed lines, adjusted p value = 0.05; vertical dashed lines, Log2FC = 1.5.

Adjusted p values are the results of Wald tests as implemented in DEseq2.

See also Figure S3 and Data S1, S2, and S3.

were modestly and inconsistently upregulated by DAV infection (Figure S3C).

Relish, the sole nuclear factor κB (NF-κB) transcription factor of the IMD pathway, can be activated through a second signaling cascade resembling the vertebrate cyclic GMP-AMP synthase (cGAS) stimulator of interferon genes (STING) pathway.[48–51] This cascade, referred to here as Sting-Relish signaling, regulates the transcription of genes distinct from those regulated by IMD signaling.[48] Several targets of Sting-Relish signaling were upregulated by DAV infection in midguts from CR and GF flies at 6 and 12 dpi (Figures 4D and S3D; Data S2).
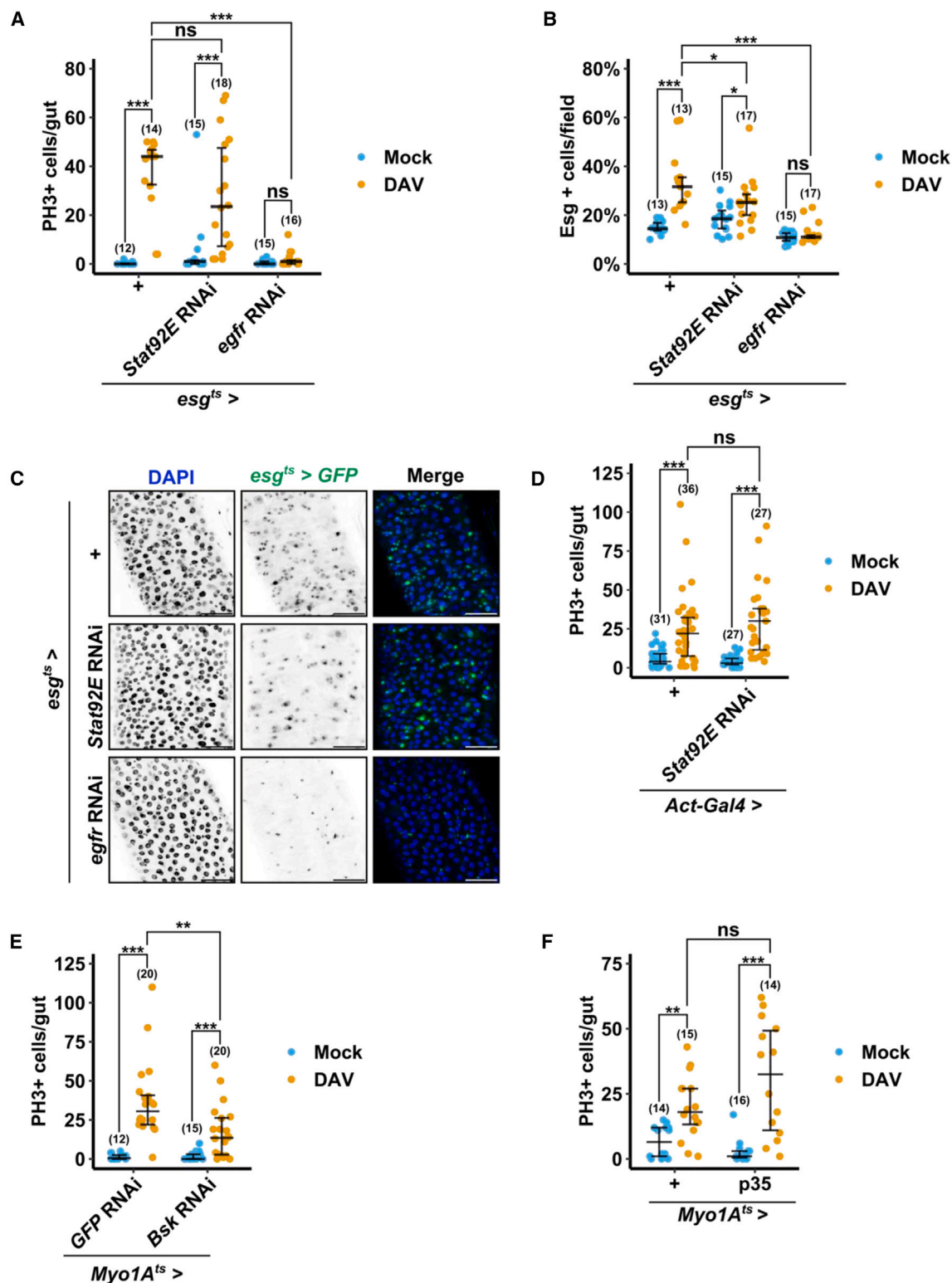
Figure 5. EGFR and JNK signaling, but not JAK-STAT signaling, play roles in DAV-induced ISC proliferation

(A) Quantification of PH3+ cells at 8 dpi in midguts from mock-infected or DAV-infected flies of the indicated genotypes.

(B) Quantification of Esg+ cells in R4 midgut regions at 8 dpi from mock-infected or DAV-infected flies of the indicated genotypes.

(C) Representative images of Esg+ cells at 8 dpi in R4 midgut regions from mock-infected or DAV-infected flies of the indicated genotypes. Scale bars, 50 μm.

(legend continued on next page)

DAV-induced ISC proliferation requires EGFR but not JAK-STAT signaling

Our RNA-seq results indicated that DAV infection upregulates canonical epithelial repair pathways in the intestine (Figure 4). We thus examined whether the mechanism of DAV-induced ISC proliferation is consistent with other stress-induced proliferative responses. We first depleted EGFR or JAK-STAT signaling in progenitors using esg^{ts} to express RNAi constructs targeting $egfr$, the gene encoding the receptor of the EGFR pathway, or $Stat92e$, the gene encoding the sole transcription factor of the JAK-STAT pathway. Progenitor-specific depletion of EGFR, but not JAK-STAT signaling, blocked DAV-induced ISC proliferation and accumulation of Esg+ cells at 8 dpi without impacting viral RNA levels (Figures 5A–5C, S4A, and S4B). Progenitor-specific depletion of JAK-STAT signaling reduced DAV-induced ISC proliferation compared with controls (Figure 5A), but the difference was not statistically significant. As a control for depletion of progenitor JAK-STAT activity, we infected flies with $Erwinia carotovora 15$ ($Ecc15$), observing a significant decrease in the ISC proliferative response to infection with this pathogenic bacterium (Figure S4C). This indicates that the minimal impact of JAK-STAT depletion in progenitors on DAV-induced ISC proliferation was not due to ineffective suppression of JAK-STAT signaling in this system. Because paracrine JAK-STAT signaling can regulate ISC proliferation non-cell autonomously,[52–54] we ubiquitously expressed $Stat92e$ RNAi using an $Actin-Gal4$ driver ($Act-Gal4$). Despite a $Stat92e$ silencing efficiency of ~84% (Figure S4D), ubiquitous depletion of JAK-STAT signaling did not significantly impact DAV-induced ISC proliferation or DAV RNA levels (Figures 5D and S4E). Moreover, $Upd3$ mutants exhibited similar levels of DAV-induced ISC proliferation and DAV RNA as their isogenic wild-type counterparts (Figures S4F and S4G). These results demonstrate that cell-autonomous EGFR signaling is required for DAV-induced ISC proliferation and do not support a role for JAK-STAT signaling in the proliferative response to DAV.

JNK signaling in ECs regulates DAV-induced ISC proliferation in an apoptosis- and JAK-STAT-independent manner

To test a potential role for EC JNK activity in regulating DAV-induced ISC proliferation, we depleted JNK signaling in ECs by expressing an RNAi construct targeting the gene encoding Bsk. Using the temperature-sensitive, EC-specific $Myo1A-Gal4$ $tubGal80^{ts}$ system (referred to as $Myo1A^{ts}$)[16] to express Bsk RNAi in ECs, we found that inhibition of EC JNK signaling did not prevent DAV-induced ISC proliferation but did significantly reduce levels of ISC proliferation compared with controls without impacting DAV RNA levels (Figures 5E and S4H).

Apoptosis is a conserved antiviral mechanism and JNK-dependent apoptosis can trigger compensatory ISC proliferation in the $D. melanogaster$ midgut.[55,56] However, a role for apoptosis in restricting enteric viral infections in $D. melanogaster$ has not been explored. Immunofluorescence with an antibody against cleaved

Dcp1 did not indicate an increase in the number of apoptotic cells in the guts of DAV-infected flies compared with mock-infected controls (data not shown). However, our RNA-seq data indicated that genes associated with apoptosis and other cell death pathways were modestly upregulated by DAV infection (Data S3). Thus, we overexpressed the caspase inhibitor, p35,[57] using $Myo1A^{ts}$ to determine if EC apoptosis plays a role in DAV-induced ISC proliferation or restricting DAV infection. ISC proliferation levels were not significantly different in DAV-infected flies overexpressing p35 in ECs compared with controls (Figure 5F), indicating that the regulatory role of JNK on DAV-induced ISC proliferation is independent of caspase activity in ECs. Arguing against an antiviral role for caspase-dependent EC apoptosis during DAV infection, overexpressing p35 in ECs did not impact the relative median survival of DAV-infected flies and reduced levels of DAV RNA compared with controls (Figures S4I–S4K). Our results indicate that JNK activity in ECs regulates DAV-induced ISC proliferation but that JAK-STAT signaling, Upd3, and caspase-dependent EC apoptosis are dispensable for the role of the JNK pathway in this context.

Sting-Relish and IMD signaling are required for DAV-induced ISC proliferation

Our results suggested that DAV infection induces ISC proliferation through mechanisms that overlap with but are incompletely described by canonical proliferative stress responses. Because NF-κB signaling is upregulated in DAV-infected midguts (Figures 4D, S3B, and S3D), we infected flies with mutations in $Relish$ ($Relish^{E20}$, referred to as $Relish$ $(−/−)$[58]) or Dif (Dif^1, referred to as Dif $(−/−)$[59]) to determine if the IMD or Toll pathways, respectively, play roles in DAV-induced ISC proliferation. Absence of Relish abrogated DAV-induced ISC proliferation at 8 dpi despite higher DAV RNA levels in $Relish$ mutants compared with isogenic wild-type flies (w^{1118}, referred to as $WT^{iso:Relish}$) (Figures 6A and S5A). DAV-infected Dif mutants exhibited elevated ISC proliferation compared with mock-infected controls but significantly less than DAV-infected isogenic wild-type flies (w^{1118}, referred to as $WT^{iso:Dif}$), and there were no significant differences in DAV RNA levels between Dif mutants and wild-type flies (Figures S5B and S5C). In agreement with a previous report,[60] $Relish$ mutants had reduced lifespans compared with wild-type flies, with substantial mortality observed by 8 dpi (Figure S5D). We thus measured ISC proliferation at 4 dpi, a time preceding mortality onset in $Relish$ mutants, to rule out the possibility that the lack of a proliferative response to DAV in these flies was an artifact of the sampling time. The absence of Relish prevented DAV-induced ISC proliferation at this earlier time point (Figure S5E). These results suggest that NF-κB signaling plays a role in DAV-induced ISC proliferation, with a particular requirement for Relish.

Relish regulates both IMD- and Sting-dependent transcriptional responses. We thus infected $Sting$ mutants ($dSTING^{Rxn}$, referred to as $Sting$ $(−/−)$[48]) or Imd mutants (Imd^1, referred to

(D–F) Quantification of PH3+ cells at 8 dpi in midguts from mock-infected or DAV-infected flies of the indicated genotypes.
Error bars indicate median with 1st and 3rd quartiles. Results were compared by two-way ANOVA with Turkey's multiple comparisons tests; ns, non-significant; *$p < 0.05$; **$p < 0.01$; ***$p < 0.001$. Numbers of biological replicates indicated in parentheses.
See also Figure S4.
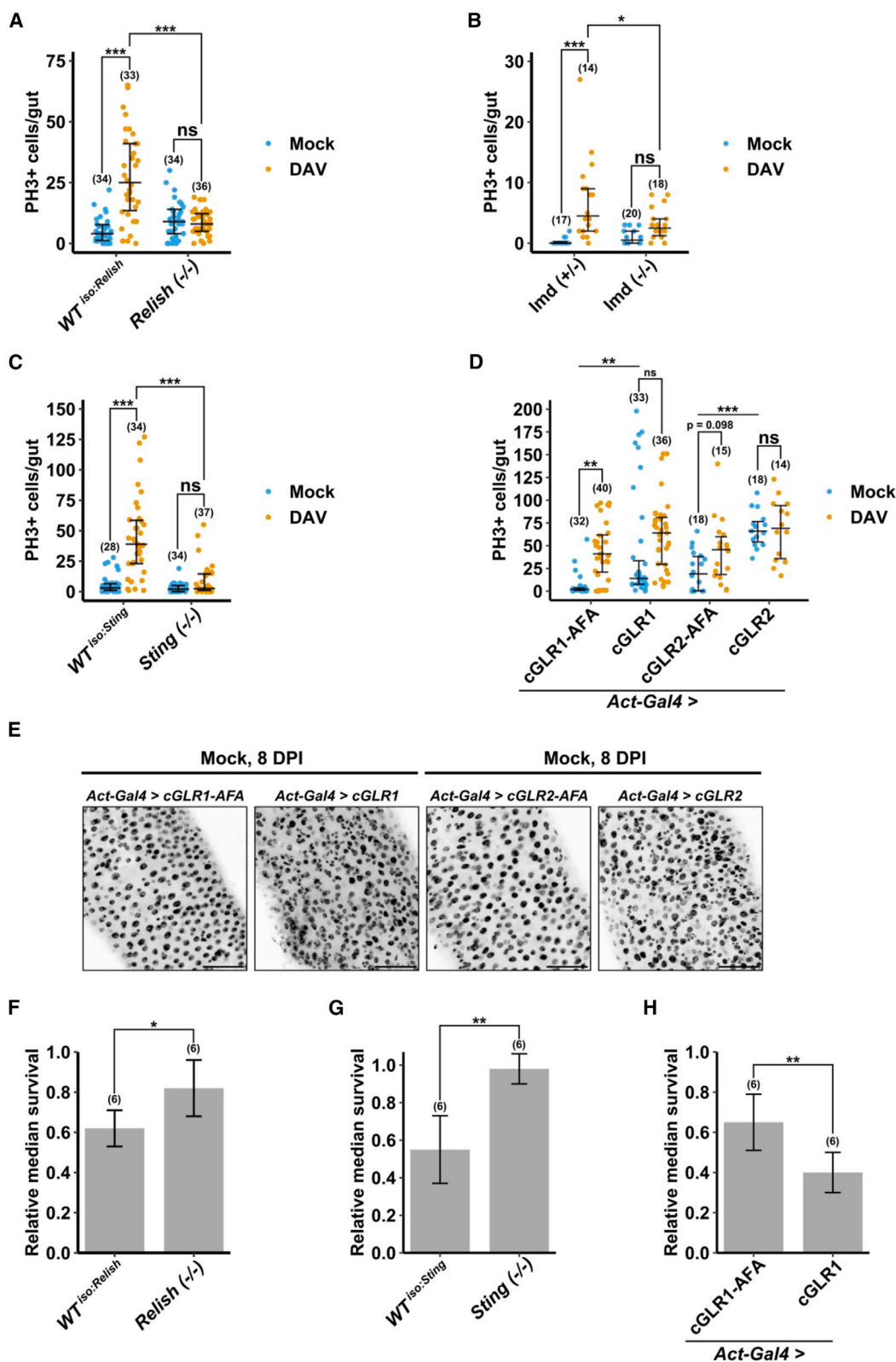
Figure 6. Sting-Relish signaling is required for DAV-induced ISC proliferation

(A–D) Quantification of PH3+ cells at 8 dpi in midguts from mock-infected or DAV-infected flies of the indicated genotypes.

(E) Representative images of DAPI-stained R4 midgut regions at 8 dpi from mock-infected flies of the indicated genotypes. Scale bars, 50 μm.

(legend continued on next page)

as *Imd (−/−)*[61]) to investigate the relative contributions of Sting-Relish and IMD signaling, respectively, to Relish-dependent DAV-induced ISC proliferation. DAV infection did not induce ISC proliferation in homozygous *Imd* or *Sting* mutants at 8 dpi (Figures 6B and 6C). As expected, wild-type flies with an isogenic genetic background relative to *Sting* mutants (referred to as *WT^iso:Sting*) exhibited high levels of DAV-induced ISC proliferation (Figure 6C). Because isogenic flies with a wild-type background relative to our *Imd* mutants were unavailable, we compared ISC proliferation in homozygous *Imd* mutants with heterozygous *Imd* mutants (referred to as *Imd (+/−)*). Although we did observe significant DAV-induced ISC proliferation in heterozygous *Imd* mutants (Figure 6B), the level of DAV-induced ISC proliferation in these flies was substantially lower than what we typically observe in wild-type flies (compare with Figure 2A). This result is consistent with a requirement for Imd in DAV-induced ISC proliferation, with increasingly reduced gene dosages correlated with increasingly lower levels of DAV-induced ISC proliferation. DAV RNA levels were similar in *Sting (−/−)* flies compared with *WT^iso:Sting* flies and in *Imd (−/−)* flies compared with *Imd (+/−)* flies (Figures S5F and S5G). Additionally, ISC proliferation was induced by *Ecc15* infection in *Sting* mutants (Figure S5H). These results indicate that Relish is required for DAV-induced ISC proliferation and suggest that both the IMD and Sting-Relish pathways play roles in the proliferative response to DAV.

Although constitutive activation of IMD signaling in progenitors is known to promote ISC proliferation,[45] potential links between Sting-Relish signaling and ISC proliferation have not been explored. We thus focused on characterizing the role of Sting-Relish signaling in the regulation of ISC proliferation. Overexpression of cGAS-like receptor 1 (cGLR1) or cGLR2 is sufficient to activate Sting-Relish signaling *in vivo*.[50,62] Thus, to confirm the role of Sting-Relish signaling in DAV-induced ISC proliferation, we measured ISC proliferation rates in flies ubiquitously overexpressing cGLR1 or cGLR2 (*Act-Gal4* UAS-cGLR1/2[50]) compared with controls overexpressing catalytically inactive cGLR1 or cGLR2 (*Act-Gal4* UAS-cGLR1/2-AFA[50]). Mock-infected flies overexpressing active cGLR1 or cGLR2 had significantly higher ISC proliferation levels compared with mock-infected flies overexpressing catalytically inactive cGLR1 or cGLR2 and exhibited epithelial irregularities resembling DAV-induced gut hypertrophy (disorganization of epithelial cells, cell clustering, and an apparent overabundance of cells with small nuclei) (Figures 6D, 6E, and S6A). Overexpressing cGLR1 or cGLR2 did not impact DAV RNA levels (Figure S6B). Along with our finding that *Sting* knockout does not impact DAV RNA levels (Figure S5G), these data suggest that Sting-Relish signaling does not play an antiviral role during oral DAV infection. Our observations indicate that Sting-Relish signaling is required for DAV-induced ISC proliferation and is sufficient to promote ISC proliferation in the absence of infection.

Our results suggested that DAV infection may reduce lifespan by promoting sustained ISC over-proliferation, thus accelerating the onset of age-dependent intestinal pathology (Figures 2, 3, and S1). If the reduced lifespan of DAV-infected flies is driven by ISC proliferation, precluding the proliferative response to DAV should prolong lifespan. Because DAV infection does not induce ISC proliferation in *Relish* or *Sting* mutants, we compared the relative median survival of DAV-infected *Relish* or *Sting* mutants with their wild-type counterparts. Indeed, the relative median survival of DAV-infected *Relish* or *Sting* mutants was significantly prolonged compared with wild-type flies, suggesting that Sting-Relish signaling may drive mortality during DAV infection (Figures 6F, 6G, S5D, and S5I). In agreement with this possibility, ectopic activation of Sting-Relish signaling by overexpression of cGLR1 accelerated DAV-associated mortality and significantly reduced the lifespan of mock-infected flies (Figures 6H and S6C). Notably, the impact of cGLR1 overexpression on lifespan was equivalent to that of DAV infection (Figure S6C).

Loss of Relish or Sting diminishes DAV-induced upregulation of genes involved in the mitotic cell cycle and epithelial renewal in the intestine

We sequenced midgut transcriptomes at 8 dpi in DAV- or mock-infected *Relish* or *Sting* mutants along with corresponding wild-type flies to identify differences in their transcriptional responses to DAV. Compared with midguts from wild-type flies, DAV RNA levels were significantly higher in *Relish* mutant midguts but not in *Sting* mutant midguts (Figure S7A). As expected, loss of Relish or Sting reduced DAV-induced upregulation of transcriptional targets of IMD- and Sting-Relish signaling (Figures S7B and S7C; Data S4). We identified 78 genes that were significantly upregulated by DAV infection in wild-type midguts, but not in midguts from *Relish* or *Sting* mutants (Figure 7A; Data S4). In agreement with our ISC proliferation data in the mutants, many of these genes belonged to the Gene Ontology (GO) terms, "multicellular organism development," "mitotic cell cycle," and "cell differentiation" (Figure 7A). Indeed, we observed broad upregulation of genes belonging to the GO term "mitotic cell cycle" (GO: 0000278) in the intestines of DAV-infected wild-type flies, but not in those of DAV-infected *Relish* or *Sting* mutants (Figure 7B; Data S5).

Compared with wild-type flies, the intestinal transcriptomes of DAV-infected *Relish* or *Sting* mutants exhibited diminished upregulation of genes belonging to the EGFR, JNK, or JAK-STAT pathways (Figures S7D–S7F). These results are consistent with a previous finding that ectopic activation of Sting-Relish signaling induces upregulation of several EGFR, JNK, and JAK-STAT pathway genes.[51] Together our results reveal that DAV infection induces global upregulation of genes involved in cell cycle progression, cellular differentiation, and regulation of epithelium renewal in the intestine. Loss of either Relish or Sting diminishes this transcriptional response to infection, supporting the possibility of a functional link between

---

(F–H) Relative median survival of DAV-infected flies of the indicated genotypes. Bar height indicates the average of biological replicates (n = 15–20 flies/replicate). Error bars in (A)–(D) indicate median with 1st and 3rd quartiles. Error bars in (F)–(H) indicate SD. Results were compared by two-way ANOVA with Turkey's multiple comparisons tests (A–D) or two-tailed t tests (F–H); ns, non-significant; *$p < 0.05$; **$p < 0.01$; ***$p < 0.001$. Numbers of biological replicates indicated in parentheses.

See also Figures S5 and S6.
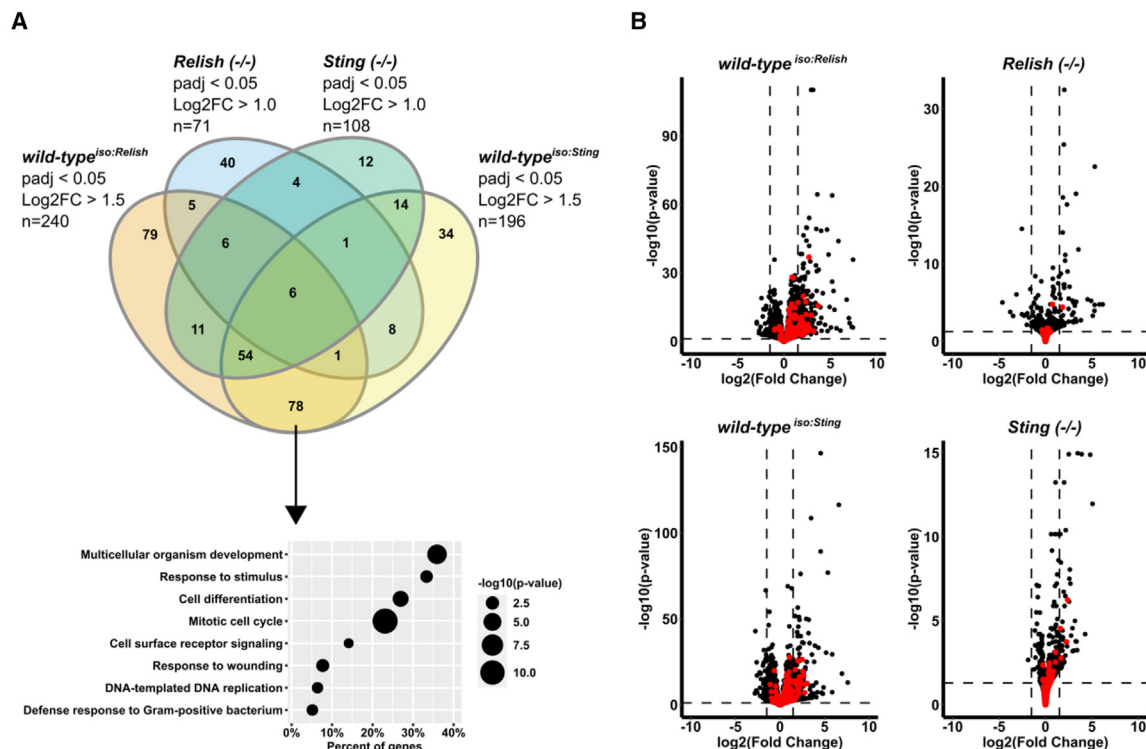
Figure 7. Loss of Relish or Sting diminishes DAV-induced upregulation of genes involved in the mitotic cell cycle and epithelial renewal in the intestine

(A) Upper: overlap of genes differentially expressed in the midguts of flies with the indicated genotypes. Log_2 fold change (Log2FC) is expression in DAV-infected/mock-infected conditions. $p$adj, adjusted p value. Lower: select GO categories of genes upregulated in wild-type flies, but not in mutants. p values are the results of Fisher's one-tailed tests as implemented in g:GOSt.[63]

(B) Expression of all genes in the indicated genotypes. Genes in the GO category mitotic cell cycle are in red (see Data S5). Expression in DAV-infected midguts/mock-infected midguts is shown. Horizontal dashed lines, adjusted p value = 0.05; vertical dashed lines, Log_2FC = 1.5. Adjusted p values are the results of Wald tests as implemented in DEseq2.[64]

See also Figure S7 and Data S4 and S5.

Sting-Relish signaling and canonical epithelial repair mechanisms during viral infection.

DISCUSSION

Here, we leveraged the *D. melanogaster* model to elucidate the physiological consequences of enteric viral infection and investigate how host-virus interactions influence infection outcomes. We found that orally acquired DAV persistently infects the adult midgut, induces sustained over-proliferation of ISCs, and accelerates age-associated intestinal pathology in a microbiota-independent manner. We observed similar phenotypes in flies persistently infected with DCV, Nora virus, or Bloomfield virus, suggesting that modulation of intestinal physiology is a common feature of viral infections. Blocking EC apoptosis did not influence the survival of infected flies and significantly reduced DAV RNA levels, arguing against an antiviral role for intestinal cell turnover. In contrast, inhibiting ISC proliferation prolonged the survival of DAV-infected flies without impacting viral RNA levels, suggesting that elevated ISC proliferation is not an adaptive host response allowing flies to resist or tolerate DAV infection but is instead a detrimental consequence of infection.

Is increased ISC proliferation beneficial for the viral infection cycle? One hypothesis is that loss of intestinal barrier function due to dysregulated cellular turnover may facilitate the dissemination of infection beyond the midgut.[65] We observed that DAV RNA levels increased in extra-intestinal tissues prior to the onset of DAV replication in the gut and this pattern was not impacted by inhibiting ISC proliferation, suggesting that the spread of DAV beyond the midgut does not depend on altered cellular turnover. Another possibility is that elevated ISC proliferation could modify epithelial composition to promote viral replication.[66] Similarly, increased ISC proliferation could conceivably facilitate changes to epithelial structure or function to promote the shedding of infectious viruses. However, our finding that *Relish* mutants exhibit higher DAV RNA levels in dissected guts compared with wild-type controls despite lacking a proliferative response to infection argues against a pro-viral role for elevated ISC proliferation. Several lines of investigation arise from our data. Does DAV infection alter the relative proportions of differentiated intestinal cell types? Are metabolic or hormonal states modulated by viral infection? Are new cells produced by DAV-induced ISC proliferation retained? Does DAV infection influence non-apoptotic epithelial cell loss, such as engulfment[67] and erebosis?[68] These questions should be addressed in future studies

and may inform conclusions regarding the functional role of virus-driven modulation of intestinal cell turnover.

Midgut RNA-seq revealed that DAV infection upregulates genes belonging to classical epithelial repair systems, including the EGFR, JAK-STAT, and JNK pathways. Knockdown experiments indicated that DAV-induced ISC proliferation requires EGFR signaling in progenitors and supported an apoptosis- and JAK-STAT-independent mitogenic role for JNK signaling in ECs during DAV infection. Intriguingly, our results uncovered a requirement for Sting-dependent NF-κB signaling in the induction of DAV-induced ISC proliferation and constitutive activation of Sting-Relish signaling was sufficient to induce ISC proliferation, promote gut hypertrophy, and reduce lifespan in the absence of infection. Experiments in cGLR loss-of-function mutants would be helpful in clarifying the homeostatic roles of Sting-Relish signaling.

Both IMD-Relish and Sting-Relish signaling play antiviral roles in *D. melanogaster*.[48–51,69–72] We observed increased DAV RNA levels in carcasses and midguts from *Relish* mutants, but not those from *Sting* mutants. Additionally, overexpression of cGLR1 did not impact DAV RNA levels or prolong the survival of infected flies. These results suggest that Relish is antiviral during DAV infection, but that its antiviral role is independent of Sting-Relish signaling in this context. Critically, these results indicate that the requirement of Sting-Relish signaling for DAV-induced ISC proliferation is not an indirect result of reduced DAV RNA levels in the mutants. Supporting our ISC proliferation data, the midguts of DAV-infected wild-type flies exhibited broad upregulation of genes involved in mitosis and cell differentiation, a response that was absent in *Relish* or *Sting* mutants. The midguts of DAV-infected *Relish* or *Sting* mutants also showed diminished upregulation of genes belonging to the EGFR, JAK-STAT, and JNK pathways compared with DAV-infected wild-type flies. Together our data suggest that Sting-Relish signaling may act upstream of or in concert with classical epithelial repair pathways to promote ISC proliferation.

Sting-dependent Relish activation upregulates genes distinct from those upregulated by the IMD-Relish pathway,[48] suggesting that Sting-Relish and IMD-Relish signaling may engage different factors to modify the regulatory activity of Relish and implying that the two signaling cascades have different functional outcomes. Mammalian cGAS-STING signaling induces the type I interferon (IFN-1) response, activates NF-κB signaling, and triggers non-canonical autophagy.[73] Virus-induced IFN-1 promotes stem cell proliferation in the mouse intestine, and NF-κB activity in mouse myeloid cells stimulates intestinal epithelial cell proliferation.[74,75] Moreover, cGAS-STING-dependent IFN-β is required for compensatory ISC proliferation following acute radiation damage in mice.[76] Thus, investigation of inflammatory cGAS-STING and Sting-Relish signaling represent promising avenues to explore how host-microbe interactions modulate cellular turnover.

Persistent viral infections are common in arthropods and are generally considered to pose no or only minor fitness costs for the host,[27] but there is relatively little published experimental data to support this claim and emerging studies demonstrate significant fitness impacts of persistent viral infection in *D. melanogaster*.[77,78] Moreover, re-analyses of published RNA-seq data from laboratory-reared flies revealed previously undetected infections with several viruses that induced significant changes in the host transcriptome.[28,35] Here, we found that persistent infections with DAV, DCV, Nora virus, or Bloomfield virus reduce lifespan, promote ISC proliferation, and are associated with intestinal dysplasia. Together these results highlight that persistent viral infections can have significant phenotypic impacts and raise the possibility that undetected viral infections may have influenced previous studies. In particular, we note that the microbiota-driven model of aging in *D. melanogaster* is based on experiments in which the commensal microbiota was ablated by embryo dechorionation.[15,18] Because this treatment also clears persistently infecting viruses,[79] one cannot exclude the possibility that viral infection may have contributed to aging phenotypes previously ascribed solely to commensal dysbiosis. Given the prevalence of persistent viral infection in laboratory flies and our observation that such infections can produce age-associated changes in the intestine, the potential contribution of viral infection to classical aging phenotypes should be studied in detail.

Our data reveal that persistent viral infection reduces lifespan by driving intestinal dysfunction in a manner involving sustained over-proliferation of ISCs. We propose that DAV infection accelerates aging by stimulating prolonged activation of inflammatory Sting-Relish signaling, resulting in dysregulation of classical epithelial repair systems and loss of intestinal homeostasis. Further studies are needed to elucidate the functional impacts of virus-driven modulation of epithelial turnover and to clarify the relationship between Sting-Relish signaling and epithelial repair. Ultimately our results uncover wide-ranging impacts of viral infection on intestinal physiology and highlight novel host-virus interactions at the intersection of immune signaling, physiology, and aging.

STAR★METHODS

Detailed methods are provided in the online version of this paper and include the following:

- KEY RESOURCES TABLE
- RESOURCE AVAILABILITY
  - Lead contact
  - Materials availability
  - Data and code availability
- EXPERIMENTAL MODEL AND STUDY PARTICIPANT DETAILS
  - Generation of persistently infected flies
- METHOD DETAILS
  - Viral infections
  - Ecc15 infections
  - Antibody production
  - Viral stock preparation and titration
  - RNA extraction and RT-qPCR
  - Survival analysis
  - Smurf assay
  - RNA FISH, immunofluorescence, and imaging
  - RNA-seq analysis
  - Gene Ontology enrichment analysis
- QUANTIFICATION AND STATISTICAL ANALYSIS

SUPPLEMENTAL INFORMATION

Supplemental information can be found online at https://doi.org/10.1016/j.cub.2024.05.009.

AUTHOR CONTRIBUTIONS

J.C.N., M.C.-S., V.M., X.G., A.J.B., and M.-C.S. designed the experiments. J.C.N., M.C.-S., and H.B. performed the experiments. J.C.N., M. Castelló-Sanjuán, L.F., M.-C Saleh, and A.J.B. analyzed the data. J.C.N., A.J.B., and M.-C.S. wrote the paper. All authors reviewed and approved the final version of the manuscript.

DECLARATION OF INTERESTS

The authors declare no competing interests.

REFERENCES

1. Zhang, P., and Edgar, B.A. (2022). Insect gut regeneration. Cold Spring Harb. Perspect. Biol. *14*, a040915. https://doi.org/10.1101/cshperspect.a040915.

2. Palikuqi, B., Rispal, J., and Klein, O. (2022). Good neighbors: The niche that fine tunes mammalian intestinal regeneration. Cold Spring Harb. Perspect. Biol. *14*, a040865. https://doi.org/10.1101/cshperspect.a040865.

3. Boumard, B., and Bardin, A.J. (2021). An amuse-bouche of stem cell regulation: Underlying principles and mechanisms from adult Drosophila intestinal stem cells. Curr. Opin. Cell Biol. *73*, 58–68. https://doi.org/10.1016/j.ceb.2021.05.007.

4. Rera, M., Clark, R.I., and Walker, D.W. (2012). Intestinal barrier dysfunction links metabolic and inflammatory markers of aging to death in Drosophila. Proc. Natl. Acad. Sci. USA *109*, 21528–21533. https://doi.org/10.1073/pnas.1215849110.

5. Turpin, W., Lee, S.-H., Raygoza Garay, J.A.R., Madsen, K.L., Meddings, J.B., Bedrani, L., Power, N., Espin-Garcia, O., Xu, W., Smith, M.I., et al. (2020). Increased intestinal permeability is associated with later development of Crohn's disease. Gastroenterology *159*, 2092–2100.e5. https://doi.org/10.1053/j.gastro.2020.08.005.

6. Ramadan, R., van Driel, M.S., Vermeulen, L., and van Neerven, S.M. (2022). Intestinal stem cell dynamics in homeostasis and cancer. Trends Cancer *8*, 416–425. https://doi.org/10.1016/j.trecan.2022.01.011.

7. Vereecke, L., Beyaert, R., and van Loo, G. (2011). Enterocyte death and intestinal barrier maintenance in homeostasis and disease. Trends Mol. Med. *17*, 584–593. https://doi.org/10.1016/j.molmed.2011.05.011.

8. Clark, R.I., and Walker, D.W. (2018). Role of gut microbiota in aging-related health decline: insights from invertebrate models. Cell. Mol. Life Sci. *75*, 93–101. https://doi.org/10.1007/s00018-017-2671-1.

9. Biteau, B., Karpac, J., Supoyo, S., DeGennaro, M., Lehmann, R., and Jasper, H. (2010). Lifespan extension by preserving proliferative homeostasis in Drosophila. PLoS Genet. *6*, e1001159. https://doi.org/10.1371/journal.pgen.1001159.

10. Funk, M.C., Zhou, J., and Boutros, M. (2020). Ageing, metabolism and the intestine. EMBO Rep. *21*, e50047. https://doi.org/10.15252/embr.202050047.

11. Li, H., and Jasper, H. (2016). Gastrointestinal stem cells in health and disease: from flies to humans. Dis. Model. Mech. *9*, 487–499. https://doi.org/10.1242/dmm.024232.

12. Ohlstein, B., and Spradling, A. (2006). The adult Drosophila posterior midgut is maintained by pluripotent stem cells. Nature *439*, 470–474. https://doi.org/10.1038/nature04333.

13. Micchelli, C.A., and Perrimon, N. (2006). Evidence that stem cells reside in the adult Drosophila midgut epithelium. Nature *439*, 475–479. https://doi.org/10.1038/nature04371.

14. Zeng, X., and Hou, S.X. (2015). Enteroendocrine cells are generated from stem cells through a distinct progenitor in the adult Drosophila posterior midgut. Development *142*, 644–653. https://doi.org/10.1242/dev.113357.

15. Buchon, N., Broderick, N.A., Chakrabarti, S., and Lemaitre, B. (2009). Invasive and indigenous microbiota impact intestinal stem cell activity through multiple pathways in Drosophila. Genes Dev. *23*, 2333–2344. https://doi.org/10.1101/gad.1827009.

16. Jiang, H., Patel, P.H., Kohlmaier, A., Grenley, M.O., McEwen, D.G., and Edgar, B.A. (2009). Cytokine/Jak/Stat signaling mediates regeneration and homeostasis in the Drosophila midgut. Cell *137*, 1343–1355. https://doi.org/10.1016/j.cell.2009.05.014.

17. Biteau, B., Hochmuth, C.E., and Jasper, H. (2008). JNK activity in somatic stem cells causes loss of tissue homeostasis in the aging Drosophila gut. Cell Stem Cell *3*, 442–455. https://doi.org/10.1016/j.stem.2008.07.024.

18. Guo, L., Karpac, J., Tran, S.L., and Jasper, H. (2014). PGRP-SC2 promotes gut immune homeostasis to limit commensal dysbiosis and extend lifespan. Cell *156*, 109–122. https://doi.org/10.1016/j.cell.2013.12.018.

19. Clark, R.I., Salazar, A., Yamada, R., Fitz-Gibbon, S., Morselli, M., Alcaraz, J., Rana, A., Rera, M., Pellegrini, M., Ja, W.W., et al. (2015). Distinct shifts in microbiota composition during Drosophila aging impair intestinal function and drive mortality. Cell Rep. *12*, 1656–1667. https://doi.org/10.1016/j.celrep.2015.08.004.

20. Li, H., Qi, Y., and Jasper, H. (2016). Ubx dynamically regulates Dpp signaling by repressing Dad expression during copper cell regeneration in the adult Drosophila midgut. Dev. Biol. *419*, 373–381. https://doi.org/10.1016/j.ydbio.2016.08.027.

21. Li, H., Qi, Y., and Jasper, H. (2016). Preventing age-related decline of gut compartmentalization limits microbiota dysbiosis and extends lifespan. Cell Host Microbe *19*, 240–253. https://doi.org/10.1016/j.chom.2016.01.008.

22. Jasper, H. (2020). Intestinal stem cell aging: origins and interventions. Annu. Rev. Physiol. *82*, 203–226. https://doi.org/10.1146/annurev-physiol-021119-034359.

23. Wu, A., Yu, B., Zhang, K., Xu, Z., Wu, D., He, J., Luo, J., Luo, Y., Yu, J., Zheng, P., et al. (2020). Transmissible gastroenteritis virus targets Paneth cells to inhibit the self-renewal and differentiation of Lgr5 intestinal stem cells via Notch signaling. Cell Death Dis. *11*, 40. https://doi.org/10.1038/s41419-020-2233-6.

24. Metzger, R.N., Krug, A.B., and Eisenächer, K. (2018). Enteric virome sensing—its role in intestinal homeostasis and immunity. Viruses *10*, 146. https://doi.org/10.3390/v10040146.

25. Adiliaghdam, F., Amatullah, H., Digumarthi, S., Saunders, T.L., Rahman, R.-U., Wong, L.P., Sadreyev, R., Droit, L., Paquette, J., Goyette, P., et al. (2022). Human enteric viruses autonomously shape inflammatory bowel disease phenotype through divergent innate immunomodulation. Sci. Immunol. *7*, eabn6660. https://doi.org/10.1126/sciimmunol.abn6660.

26. Epple, H.J., Allers, K., Tröger, H., Kühl, A., Erben, U., Fromm, M., Zeitz, M., Loddenkemper, C., Schulzke, J.D., and Schneider, T. (2010). Acute HIV infection induces mucosal infiltration with CD4+ and CD8+ T cells, epithelial apoptosis, and a mucosal barrier defect. Gastroenterology *139*, 1289–1300. https://doi.org/10.1053/j.gastro.2010.06.065.

27. Goic, B., and Saleh, M.-C. (2012). Living with the enemy: viral persistent infections from a friendly viewpoint. Curr. Opin. Microbiol. *15*, 531–537. https://doi.org/10.1016/j.mib.2012.06.002.

28. Kuyateh, O., and Obbard, D.J. (2023). Viruses in laboratory Drosophila and their impact on host gene expression. Viruses *15*, 1849. https://doi.org/10.3390/v15091849.

29. Webster, C.L., Waldron, F.M., Robertson, S., Crowson, D., Ferrari, G., Quintana, J.F., Brouqui, J.-M., Bayne, E.H., Longdon, B., Buck, A.H., et al. (2015). The discovery, distribution, and evolution of viruses associated with Drosophila melanogaster. PLoS Biol. *13*, e1002210. https://doi.org/10.1371/journal.pbio.1002210.

30. Ferreira, Á.G., Naylor, H., Esteves, S.S., Pais, I.S., Martins, N.E., and Teixeira, L. (2014). The Toll-dorsal pathway is required for resistance to viral oral infection in Drosophila. PLoS Pathog. *10*, e1004507. https://doi.org/10.1371/journal.ppat.1004507.

31. Habayeb, M.S., Ekengren, S.K., and Hultmark, D. (2006). Nora virus, a persistent virus in Drosophila, defines a new picorna-like virus family. J. Gen. Virol. *87*, 3045–3051. https://doi.org/10.1099/vir.0.81997-0.

32. Cross, S.T., Maertens, B.L., Dunham, T.J., Rodgers, C.P., Brehm, A.L., Miller, M.R., Williams, A.M., Foy, B.D., and Stenglein, M.D. (2020). Partitiviruses infecting Drosophila melanogaster and Aedes aegypti exhibit efficient biparental vertical transmission. J. Virol. *94*, 10. https://doi.org/10.1128/JVI.01070-20.

33. Ambrose, R.L., Lander, G.C., Maaty, W.S., Bothner, B., Johnson, J.E., and Johnson, K.N. (2009). Drosophila A virus is an unusual RNA virus with a T= 3 icosahedral core and permuted RNA-dependent RNA polymerase. J. Gen. Virol. *90*, 2191–2200. https://doi.org/10.1099/vir.0.012104-0.

34. Brosh, O., Fabian, D.K., Cogni, R., Tolosana, I., Day, J.P., Olivieri, F., Merckx, M., Akilli, N., Szkuta, P., and Jiggins, F.M. (2022). A novel transposable element-mediated mechanism causes antiviral resistance in Drosophila through truncating the Veneno protein. Proc. Natl. Acad. Sci. USA *119*, e2122026119. https://doi.org/10.1073/pnas.2122026119.

35. Silva, J.M.F., Nagata, T., Melo, F.L., and Elena, S.F. (2021). Heterogeneity in the Response of Different Subtypes of Drosophila melanogaster Midgut Cells to Viral Infections. Viruses *13*, 2284. https://doi.org/10.3390/v13112284.

36. Nigg, J.C., Mongelli, V., Blanc, H., and Saleh, M.-C. (2022). Innovative Toolbox for the Quantification of Drosophila C Virus, Drosophila A Virus, and Nora Virus. J. Mol. Biol. *434*, 167308. https://doi.org/10.1016/j.jmb.2021.167308.

37. Ohlstein, B., and Spradling, A. (2007). Multipotent Drosophila intestinal stem cells specify daughter cell fates by differential notch signaling. Science *315*, 988–992. https://doi.org/10.1126/science.1136606.

38. Sasaki, A., Nishimura, T., Takano, T., Naito, S., and Yoo, S.K. (2021). white regulates proliferative homeostasis of intestinal stem cells during ageing in Drosophila. Nat. Metab. *3*, 546–557. https://doi.org/10.1038/s42255-021-00375-x.

39. Sheng, X., Zhu, Y., Zhou, J., Yan, L., Du, G., Liu, Z., and Chen, H. (2021). Antioxidant effects of caffeic acid lead to protection of drosophila intestinal stem cell aging. Front. Cell Dev. Biol. *9*, 735483. https://doi.org/10.3389/fcell.2021.735483.

40. Choi, N.H., Kim, J.G., Yang, D.J., Kim, Y.S., and Yoo, M.A. (2008). Age-related changes in Drosophila midgut are associated with PVF2, a PDGF/VEGF-like growth factor. Aging Cell *7*, 318–334. https://doi.org/10.1111/j.1474-9726.2008.00380.x.

41. Salazar, A.M., Aparicio, R., Clark, R.I., Rera, M., and Walker, D.W. (2023). Intestinal barrier dysfunction: an evolutionarily conserved hallmark of aging. Dis. Model. Mech. *16*, dmm049969. https://doi.org/10.1242/dmm.049969.

42. Jin, Y., Patel, P.H., Kohlmaier, A., Pavlovic, B., Zhang, C., and Edgar, B.A. (2017). Intestinal stem cell pool regulation in Drosophila. Stem Cell Rep. *8*, 1479–1487. https://doi.org/10.1016/j.stemcr.2017.04.002.

43. Wang, L., Zeng, X., Ryoo, H.D., and Jasper, H. (2014). Integration of UPRER and oxidative stress signaling in the control of intestinal stem cell proliferation. PLoS Genet. *10*, e1004568. https://doi.org/10.1371/journal.pgen.1004568.

44. Buchon, N., Silverman, N., and Cherry, S. (2014). Immunity in Drosophila melanogaster—from microbial recognition to whole-organism physiology. Nat. Rev. Immunol. *14*, 796–810. https://doi.org/10.1038/nri3763.

45. Petkau, K., Ferguson, M., Guntermann, S., and Foley, E. (2017). Constitutive immune activity promotes tumorigenesis in Drosophila intestinal progenitor cells. Cell Rep. *20*, 1784–1793. https://doi.org/10.1016/j.celrep.2017.07.078.

46. Shin, M., Ferguson, M., Willms, R.J., Jones, L.O., Petkau, K., and Foley, E. (2022). Immune regulation of intestinal-stem-cell function in Drosophila. Stem Cell Rep. *17*, 741–755. https://doi.org/10.1016/j.stemcr.2022.02.009.

47. Ferguson, M., Shin, M., and Foley, E. (2022). Relish/NF-kB acts in intestinal stem cells to promote epithelial repair in Drosophila. bioRxiv, 2022–2029.

48. Goto, A., Okado, K., Martins, N., Cai, H., Barbier, V., Lamiable, O., Troxler, L., Santiago, E., Kuhn, L., and Paik, D. (2018). The kinase IKKβ regulates a STING- and NF-κB-dependent antiviral response pathway in Drosophila. Immunity *49*, 225–234.e4.

49. Slavik, K.M., Morehouse, B.R., Ragucci, A.E., Zhou, W., Ai, X., Chen, Y., Li, L., Wei, Z., Bähre, H., König, M., et al. (2021). cGAS-like receptors sense RNA and control 3′ 2′-cGAMP signalling in Drosophila. Nature *597*, 109–113. https://doi.org/10.1038/s41586-021-03743-5.

50. Holleufer, A., Winther, K.G., Gad, H.H., Ai, X., Chen, Y., Li, L., Wei, Z., Deng, H., Liu, J., Frederiksen, N.A., et al. (2021). Two cGAS-like receptors induce antiviral immunity in Drosophila. Nature *597*, 114–118. https://doi.org/10.1038/s41586-021-03800-z.

51. Cai, H., Holleufer, A., Simonsen, B., Schneider, J., Lemoine, A., Gad, H.H., Huang, J., Huang, J., Chen, D., Peng, T., et al. (2020). 2′ 3′-cGAMP triggers a STING-and NF-κB–dependent broad antiviral response in Drosophila. Sci. Signal. *13*, eabc4537. https://doi.org/10.1126/scisignal.abc4537.

52. Buchon, N., Broderick, N.A., Kuraishi, T., and Lemaitre, B. (2010). Drosophila EGFR pathway coordinates stem cell proliferation and gut re-modeling following infection. BMC Biol. *8*, 152. https://doi.org/10.1186/1741-7007-8-152.

53. Jiang, H., Grenley, M.O., Bravo, M.-J., Blumhagen, R.Z., and Edgar, B.A. (2011). EGFR/Ras/MAPK signaling mediates adult midgut epithelial homeostasis and regeneration in Drosophila. Cell Stem Cell *8*, 84–95. https://doi.org/10.1016/j.stem.2010.11.026.

54. Zhou, F., Rasmussen, A., Lee, S., and Agaisse, H. (2013). The UPD3 cytokine couples environmental challenge and intestinal stem cell division through modulation of JAK/STAT signaling in the stem cell microenvironment. Dev. Biol. *373*, 383–393. https://doi.org/10.1016/j.ydbio.2012.10.023.

55. Liang, J., Balachandra, S., Ngo, S., and O'Brien, L.E. (2017). Feedback regulation of steady-state epithelial turnover and organ size. Nature *548*, 588–591. https://doi.org/10.1038/nature23678.

56. Mussabekova, A., Daeffler, L., and Imler, J.-L. (2017). Innate and intrinsic antiviral immunity in Drosophila. Cell. Mol. Life Sci. *74*, 2039–2054. https://doi.org/10.1007/s00018-017-2453-9.

57. Clem, R.J., Fechheimer, M., and Miller, L.K. (1991). Prevention of apoptosis by a baculovirus gene during infection of insect cells. Science *254*, 1388–1390. https://doi.org/10.1126/science.1962198.

58. Hedengren, M., Asling, B., Dushay, M.S., Ando, I., Ekengren, S., Wihlborg, M., and Hultmark, D. (1999). Relish, a central factor in the control of humoral but not cellular immunity in Drosophila. Mol. Cell *4*, 827–837. https://doi.org/10.1016/s1097-2765(00)80392-5.

59. Rutschmann, S., Jung, A.C., Hetru, C., Reichhart, J.-M., Hoffmann, J.A., and Ferrandon, D. (2000). The Rel protein DIF mediates the antifungal but not the antibacterial host defense in Drosophila. Immunity *12*, 569–580. https://doi.org/10.1016/S1074-7613(00)80208-3.

60. Iatsenko, I., Boquete, J.-P., and Lemaitre, B. (2018). Microbiota-derived lactate activates production of reactive oxygen species by the intestinal

NADPH oxidase Nox and shortens Drosophila lifespan. Immunity *49*, 929–942.e5. https://doi.org/10.1016/j.immuni.2018.09.017.

61. Lemaitre, B., Kromer-Metzger, E., Michaut, L., Nicolas, E., Meister, M., Georgel, P., Reichhart, J.M., and Hoffmann, J.A. (1995). A recessive mutation, immune deficiency (imd), defines two distinct control pathways in the Drosophila host defense. Proc. Natl. Acad. Sci. USA *92*, 9465–9469. https://doi.org/10.1073/pnas.92.21.9465.

62. Cai, H., Li, L., Slavik, K.M., Huang, J., Yin, T., Ai, X., Hédelin, L., Haas, G., Xiang, Z., Yang, Y., et al. (2023). The virus-induced cyclic dinucleotide 2′3′-c-di-GMP mediates STING-dependent antiviral immunity in Drosophila. Immunity *56*, 1991–2005.e9. https://doi.org/10.1016/j.immuni.2023.08.006.

63. Kolberg, L., Raudvere, U., Kuzmin, I., Adler, P., Vilo, J., and Peterson, H. (2023). g: Profiler—interoperable web service for functional enrichment analysis and gene identifier mapping (2023 update). Nucleic Acids. Res. *51*, W207–W212.

64. Love, M.I., Huber, W., and Anders, S. (2014). Moderated estimation of fold change and dispersion for RNA-seq data with DESeq2. Genome Biol. *15*, 550. https://doi.org/10.1186/s13059-014-0550-8.

65. Carpenter, A., and Clem, R.J. (2023). Factors Affecting Arbovirus Midgut Escape in Mosquitoes. Pathogens *12*, 220. https://doi.org/10.3390/pathogens12020220.

66. Hixson, B., Taracena, M.L., and Buchon, N. (2021). Midgut epithelial dynamics are central to mosquitoes' physiology and fitness, and to the transmission of vector-borne disease. Front. Cell. Infect. Microbiol. *11*, 653156. https://doi.org/10.3389/fcimb.2021.653156.

67. Nainu, F., Tanaka, Y., Shiratsuchi, A., and Nakanishi, Y. (2015). Protection of insects against viral infection by apoptosis-dependent phagocytosis. J. Immunol. *195*, 5696–5706. https://doi.org/10.4049/jimmunol.1500613.

68. Ciesielski, H.M., Nishida, H., Takano, T., Fukuhara, A., Otani, T., Ikegawa, Y., Okada, M., Nishimura, T., Furuse, M., and Yoo, S.K. (2022). Erebosis, a new cell death mechanism during homeostatic turnover of gut enterocytes. PLoS Biol. *20*, e3001586. https://doi.org/10.1371/journal.pbio.3001586.

69. Costa, A., Jan, E., Sarnow, P., and Schneider, D. (2009). The Imd pathway is involved in antiviral immune responses in Drosophila. PLoS One *4*, e7436. https://doi.org/10.1371/journal.pone.0007436.

70. Dostert, C., Jouanguy, E., Irving, P., Troxler, L., Galiana-Arnoux, D., Hetru, C., Hoffmann, J.A., and Imler, J.-L. (2005). The Jak-STAT signaling pathway is required but not sufficient for the antiviral response of drosophila. Nat. Immunol. *6*, 946–953. https://doi.org/10.1038/ni1237.

71. Lamiable, O., Kellenberger, C., Kemp, C., Troxler, L., Pelte, N., Boutros, M., Marques, J.T., Daeffler, L., Hoffmann, J.A., Roussel, A., et al. (2016). Cytokine Diedel and a viral homologue suppress the IMD pathway in Drosophila. Proc. Natl. Acad. Sci. USA *113*, 698–703. https://doi.org/10.1073/pnas.1516122113.

72. Segrist, E., Dittmar, M., Gold, B., and Cherry, S. (2021). Orally acquired cyclic dinucleotides drive dSTING-dependent antiviral immunity in enterocytes. Cell Rep. *37*, 110150. https://doi.org/10.1016/j.celrep.2021.110150.

73. Sun, Z., and Hornung, V. (2022). cGAS–STING signaling. Curr. Biol. *32*, R730–R734. https://doi.org/10.1016/j.cub.2022.05.027.

74. Sun, L., Miyoshi, H., Origanti, S., Nice, T.J., Barger, A.C., Manieri, N.A., Fogel, L.A., French, A.R., Piwnica-Worms, D., Piwnica-Worms, H., et al. (2015). Type I interferons link viral infection to enhanced epithelial turnover

and repair. Cell Host Microbe *17*, 85–97. https://doi.org/10.1016/j.chom.2014.11.004.

75. Greten, F.R., Eckmann, L., Greten, T.F., Park, J.M., Li, Z.-W., Egan, L.J., Kagnoff, M.F., and Karin, M. (2004). IKKβ links inflammation and tumorigenesis in a mouse model of colitis-associated cancer. Cell *118*, 285–296. https://doi.org/10.1016/j.cell.2004.07.013.

76. Leibowitz, B.J., Zhao, G., Wei, L., Ruan, H., Epperly, M., Chen, L., Lu, X., Greenberger, J.S., Zhang, L., and Yu, J. (2021). Interferon β drives intestinal regeneration after radiation. Sci. Adv. *7*, eabi5253. https://doi.org/10.1126/sciadv.abi5253.

77. Wallace, M.A., and Obbard, D.J. (2023). Naturally occurring viruses of Drosophila reduce offspring number and lifespan. Preprint at bioRxiv.

78. Hanson, M.A., and Lemaitre, B. (2023). Antimicrobial peptides do not directly contribute to aging in Drosophila, but improve lifespan by preventing dysbiosis. Dis. Model. Mech. *16*, dmm049965. https://doi.org/10.1242/dmm.049965.

79. Merkling, S.H., and Van Rij, R.P. (2015). Analysis of resistance and tolerance to virus infection in Drosophila. Nat. Protoc. *10*, 1084–1097. https://doi.org/10.1038/nprot.2015.071.

80. Buchon, N., Broderick, N.A., Poidevin, M., Pradervand, S., and Lemaitre, B. (2009). Drosophila intestinal response to bacterial infection: activation of host defense and stem cell proliferation. Cell Host Microbe *5*, 200–211. https://doi.org/10.1016/j.chom.2009.01.003.

81. Dobin, A., Davis, C.A., Schlesinger, F., Drenkow, J., Zaleski, C., Jha, S., Batut, P., Chaisson, M., and Gingeras, T.R. (2013). STAR: ultrafast universal RNA-seq aligner. Bioinformatics *29*, 15–21. https://doi.org/10.1093/bioinformatics/bts635.

82. Putri, G.H., Anders, S., Pyl, P.T., Pimanda, J.E., and Zanini, F. (2022). Analysing high-throughput sequencing data in Python with HTSeq 2.0. Bioinformatics *38*, 2943–2945. https://doi.org/10.1093/bioinformatics/btac166.

83. RStudio Team (2020). RStudio: Integrated Development for R. RStudio, PBC, Boston, MA URL http://www.rstudio.com/.

84. Bankhead, P., Loughrey, M.B., Fernández, J.A., Dombrowski, Y., McArt, D.G., Dunne, P.D., McQuaid, S., Gray, R.T., Murray, L.J., and Coleman, H.G. (2017). QuPath: Open source software for digital pathology image analysis. Sci. Rep. *7*, 16878.

85. Mongelli, V., Lequime, S., Kousathanas, A., Gausson, V., Blanc, H., Nigg, J., Quintana-Murci, L., Elena, S.F., and Saleh, M.-C. (2022). Innate immune pathways act synergistically to constrain RNA virus evolution in Drosophila melanogaster. Nat. Ecol. Evol. *6*, 565–578. https://doi.org/10.1038/s41559-022-01697-z.

86. Reed, L.J., and Muench, H. (1938). A simple method of estimating fifty per cent endpoints. Am. J. Epidemiol. *27*, 493–497. https://doi.org/10.1093/oxfordjournals.aje.a118408.

87. Livak, K.J., and Schmittgen, T.D. (2001). Analysis of relative gene expression data using real-time quantitative PCR and the $2^{-\Delta\Delta CT}$ method. Methods *25*, 402–408. https://doi.org/10.1006/meth.2001.1262.

88. Martins, R.R., McCracken, A.W., Simons, M.J.P., Henriques, C.M., and Rera, M. (2018). How to catch a smurf? – Ageing and beyond… In vivo assessment of intestinal permeability in multiple model organisms. Bio Protoc. *8*, e2722. https://doi.org/10.21769/BioProtoc.2722.

89. (2023). SYNTAX system and software. https://dev-dnascript.pantheonsite.io/wp-content/uploads/2023/05/23DNA003_Product-Information-Sheet_Syntax-05162023-2.pdf.

STAR★METHODS

KEY RESOURCES TABLE

REAGENT or RESOURCE	SOURCE	IDENTIFIER
Antibodies		
Rabbit anti-DAV	GenScript Biotech	This study
Mouse anti-Delta (1:1000)	DSHB	Cat# c594.9b; RRID: AB_528194
Mouse anti-Prospero (1:1000)	DSHB	Cat# Prospero (MR1A); RRID: AB_528440
Rabbit antiAnti-PH3 (1:1000)	Merck Millipore	Cat# 06-570; RRID: AB_310177
Chicken anti-GFP (1:2000)	Invitrogen	Cat# A10262; RRID: AB_2534023
Goat anti-rabbit-647 (1:500)	Invitrogen	Cat# A-21244; RRID: AB_2535812
Goat anti-mouse-488 (1:500)	Invitrogen	Cat# A-11029; RRID: AB_2534088
Goat anti-chicken-488 (1:500)	Invitrogen	Cat# A32931; RRID: AB_2762843
Donkey anti-rabbit-HRP (1:2000)	Cytiva	Cat# NA934; RRID: AB_772206
Bacterial and virus strains		
Drosophila A virus	Nigg et al.[36]	N/A
Drosophila C virus	Nigg et al.[36]	N/A
Nora virus	Nigg et al.[36]	N/A
Bloomfield virus	This isolate is available upon request	This study
Erwinia carotovora carotovora 15 (Ecc15)	B. Lemaitre; Buchon et al.[80]	N/A
Chemicals, peptides, and recombinant proteins		
TRIzol	Invitrogen	Cat# 15596026
16% paraformaldehyde	Thermo Scientific	Cat# 043368.9M
Deionized formamide	Invitrogen	Cat# AM9342
FD&C Blue No.1	Thermo Scientific	Cat# 229730250
SuperScript II reverse transcriptase	Invitrogen	Cat# 18064022
RNaseOUT Recombinant Ribonuclease Inhibitor	Invitrogen	Cat# 10777019
DNase I recombinant, RNase-free	Roche	Cat# 04716728001
cOmplete EDTA-free Protease Inhibitor Cocktail	Roche	Cat# 11873580001
Critical commercial assays		
Luminaris Color HiGreen qPCR Master Mix, low ROX	Thermo Scientific	Cat# K0374
Maxima H Minus First Strand cDNA Synthesis Kit	Thermo Scientific	Cat# K1652
Qubit RNA BR Assay Kit	Invitrogen	Cat# Q10211
1-Step Turbo TMB-ELISA substrate solution	Thermo Scientific	Cat# 34022
TruSeq Stranded mRNA Library Prep kit	Illumina	Cat# 20020595
IDT for Illumina TruSeq RNA UD Indexes	Illumina	Cat# 20022371
NEBNext Ultra II RNA Library Prep Kit for Illumina	New England Biolabs	Cat# E7770L
NEBNext Multiplex Oligos for Illumina	New England Biolabs	Cat# E7600S
NextSeq 500/550 High Output Kit v2.5	Illumina	Cat# 20024907
Deposited data		
RNAseq data	This paper	SRA: PRJNA1041289
Microscopy data	This paper	Zenodo: https://doi.org/10.5281/zenodo.10079314

Continued

REAGENT or RESOURCE	SOURCE	IDENTIFIER
Experimental models: Organisms/strains		
D. melanogaster: w^{1118}	Bloomington Drosophila Stock Center	BDSC Cat# 3605; RRID: BDSC_3605
D. melanogaster: w^{1118} persistently infected with DAV	Nigg et al.[36]	N/A
D. melanogaster: w^{1118} persistently infected with DCV	Nigg et al.[36]	N/A
D. melanogaster: w^{1118} persistently infected with Nora virus	Nigg et al.[36]	N/A
D. melanogaster: w^{1118} persistently infected with Bloomfield virus	This study	N/A
D. melanogaster: esg-GAL4, tubGAL80 ts UAS-GFP	Jiang et al.[16]	N/A
D. melanogaster: esg-GAL4 UAS-GFP; Su(H) GBE-GAL80 tubGAL80 ts	Wang et al.[43]	N/A
D. melanogaster: UAS-Wee1; UAS-Dacapo	Gift from Laura Buttitta, University of Michigan, Ann Arbor, MI, USA	N/A
D. melanogaster: UAS-egfr RNAi (GD)	Vienna Drosophila Resource Center	VDRC Cat# 43267
D. melanogaster: UAS-Stat92e RNAi (GD)	Vienna Drosophila Resource Center	VDRC Cat# 43867
D. melanogaster: Act5C-GAL4	Gift from Bruno Lemaitre, École Polytechnique Fédérale de Lausanne, Switzerland	N/A
D. melanogaster: P{w[+mC]=XP}upd3[d11639]	Bloomington Drosophila Stock Center	BDSC Cat#19355; RRID: BDSC_19355
D. melanogaster: UAS-Bsk RNAi (KK)	Vienna Drosophila Resource Center	VDRC Cat# 104569
D. melanogaster: UAS-GFP RNAi (KK)	Vienna Drosophila Resource Center	VDRC Cat# 60103
D. melanogaster: MyoIA-GAL4; tubGAL80 ts UAS-GFP	Jiang et al.[16]	N/A
D. melanogaster: UAS-p35	Gift from Renata Basto, Institut Curie, Paris, France	N/A
D. melanogaster: Relish^{E20}	Hedengren et al.[58]	N/A
D. melanogaster: Dif^{1}	Rutschmann et al.[59]	N/A
D. melanogaster: Imd^{1} genotype	Lemaitre et al.[61]	BDSC Cat# 55711; RRID: BDSC_55711
D. melanogaster: dSTING^{Rxn}	Goto et al.[48]	N/A
D. melanogaster: dSTING^{control}	Goto et al.[48]	N/A
D. melanogaster: UAS-cGLR1	Holleufer et al.[50]	N/A
D. melanogaster: UAS-cGLR1-AFA	Holleufer et al.[50]	N/A
D. melanogaster: UAS-cGLR2	Holleufer et al.[50]	N/A
D. melanogaster: UAS-cGLR2-AFA	Holleufer et al.[50]	N/A
Oligonucleotides		
Oligonucleotides for RNA FISH of positive strand DAV RNA	See Table S1 for oligonucleotide sequences	N/A
DAV_tag_F: 5' AATTCAAGCTCGTCTTCCTCGG TTGGATCAGGCTAGTGTAGG	Nigg et al.[36]	N/A
DAV_qPCR_R: 5' TGCAACCGGACTCCAAGTTC	Nigg et al.[36]	N/A
Tag_qPCR_F: 5' AATTCAAGCTCGTCTTCCTCG	Nigg et al.[36]	N/A
DAV_qPCR_R: 5' GTTGGATCAGGCTAGTGTAGG	This study	N/A
Rpl32_qPCR_F: 5' CGGATCGATATGCTAAGCTGT	This study	N/A
Rpl32_qPCR_R: 5' GCGCTTGTTCGATCCGTA	This study	N/A
Stat92e qPCR_F: 5' TAAACTCCACATCCTCGCCG	This study	N/A
Stat92e qPCR_R: 5' GCCAGTTCTTGAGCTCGTGT	This study	N/A

(Continued on next page)

Continued

REAGENT or RESOURCE	SOURCE	IDENTIFIER
Software and algorithms		
STAR (version 020201)	Dobin et al.[81]	URL: https://github.com/alexdobin/STAR
HTSeq (version 0.6.1p1)	Putri et al.[82]	URL: https://htseq.readthedocs.io/en/master/index.html#
DESeq2	Love at al.[64]	URL: https://bioconductor.org/packages/release/bioc/html/DESeq2.html
RStudio (version 2023.03.1)	RStudio Team (2020)[83]	URL: https://posit.co/products/open-source/rstudio/
g:Profiler	Kolberg et al.[63]	URL: https://biit.cs.ut.ee/gprofiler/gost
ImageJ (version 1.53t)	NIH	URL: https://imagej.nih.gov/ij/
Inkscape (version 0.92)	The Inkscape Project	URL: https://inkscape.org/
Prism 9 (version 9.5.1)	GraphPad Software	RRID: SCR_002798
QuPath (version 0.4.3)	Bankhead et al.[84]	URL: https://qupath.github.io/

RESOURCE AVAILABILITY

Lead contact
Further information and requests for resources and reagents should be directed to and will be fulfilled by the lead contact, Carla Saleh (carla.saleh@pasteur.fr).

Materials availability
Materials generated in this study include persistently-infected fly stocks and an antibody against the DAV capsid protein. These are freely available without restriction from the lead contact upon request.

Data and code availability

- RNA-seq data have been deposited at SRA and are publicly available as of the date of publication. Accession numbers are listed in the key resources table. Microscopy data reported in this paper have been deposited at Zenodo and are publicly available as of the date of publication. DOIs are listed in the key resources table.
- This paper does not report original code.
- Any additional information required to reanalyze the data reported in this paper is available from the lead contact upon request.

EXPERIMENTAL MODEL AND STUDY PARTICIPANT DETAILS

All fly stocks were maintained on a standard cornmeal diet (Bloomington) at 25 °C under a 12:12 hour light:dark cycle. All fly stocks were treated to clear potential persistent viral infections as previously described.[79] Briefly, eggs were treated with 50% bleach for 10 minutes, washed three times with distilled water, and transferred to fresh vials. All fly stocks were checked for the presence of *Wolbachia* infection as previously described and, when necessary, treated to clear Wolbachia infection.[79] This was accomplished by rearing the stocks on standard cornmeal diet containing 25 mg/mL tetracycline. Absence of *Wolbachia* infection was verified in the F3 of treated flies. Unless otherwise stated, w^{1118} flies were used for all experiments. Fly stocks with mutations in *Relish* (*Relish^{E20}*), *Dif* (*Dif^1*), or *Upd3* were isogenized to the w^{1118} line genetic background by backcrossing at least ten times to the w^{1118} line as previously described.[85] Isogenized *Relish* and *Dif* mutants are the same stocks described by Mongelli et al.[85] The isogenized *Upd3* mutant and the corresponding w^{1118} wild-type stock were a gift from P. Vale (University of Edinburgh, Scotland). For Gal4-driven over-expression or RNAi experiments, virgin females containing the Gal4 driver were crossed with males containing the UAS-transgene and F1 adults (males and females together) were collected at 1-3 days of age. For experiments involving the esg^{ts}, esg^{ts}; Su(H)-Gal80, or $Myo1A^{ts}$ Gal4 driver lines, crosses were maintained at 18 °C. All other crosses were maintained at 25 °C. Gene expression or RNAi was induced by shifting flies to 29 °C 24 hours prior to infection. The effectiveness of gene silencing or overexpression was validated by RT-qPCR (data not shown). GF adult flies were generated by placing newly eclosed adults on standard cornmeal diet (Bloomington) containing 50 μg/ml ampicillin, 50 μg/ml kanamycin, and 10 μg/ml gentamycin. GF flies were maintained on the antibiotic-containing diet and flipped to fresh vials every two days. GF status was verified at 6 and 12 dpi by plating feces on LB agar plates. The fly stocks and crosses used for the experiments depicted in each figure are as follows.

Figures 1, 2A–2C, 2G, 4, S1, S2, and S3: w^{1118}
Figures 2D–2F: the F1 of esg^{ts} females crossed with w^{1118} males
Figure 3: the F1 of esg^{ts}; Su(H)-Gal80 females crossed with w^{1118} or UAS-Wee1; UAS-Dacapo males

Figures 5A–5C and S4A–S4C: the F1 of *esg*^{ts} females crossed with *w*^{1118}, UAS-Stat92e RNAi (VDRC Cat# 43867), or UAS-egfr RNAi (VDRC Cat# 43267) males

Figures 5D, S4D, and S4E: the F1 of *Act-Gal4* females crossed with UAS-Stat92e RNAi (VDRC Cat# 43867) males

Figures 5E and S4H: the F1 of *Myo1A*^{ts} females crossed with UAS-GFP RNAi (VDRC Cat# 60103) or UAS-Bsk RNAi (VDRC Cat# 104569) males

Figures 5F and S4I–S4K: the F1 of *Myo1A*^{ts} females crossed with *w*^{1118} or UAS-p35 males

Figure s 6A, 6F, S5A, S5D, and S5E: *w*^{1118} and isogenized *Relish*^{E20}

Figures 6B and S5F: Imd^1 mutants (Bloomington Cat# 55711) or the F1 of Imd^1 mutant males and *w*^{1118} females

Figure s 6C, 6G, and S5G–S5I: *dSTING*^{control} and *dSTING*^{Rxn} (gift from J.L. Imler, Université de Strasbourg, France)

Figure s 6D, 6E, 6H, and S6: the F1 of *Act-Gal4* females crossed with UAS-cGLR1/2 or UAS-cGLR1/2-AFA males (gift from J.L. Imler, Université de Strasbourg, France)

Figures 7 and S7: *w*^{1118}, isogenized *Relish*^{E20}, *dSTING*^{control}, and *dSTING*^{Rxn}

Figures S5B and S5C: *w*^{1118} and isogenized *Dif*^{1}

Figures S4F and S4G: *w*^{1118} and isogenized P{w[+mC]=XP}upd3[d11639] (BDSC Cat#19355)

Generation of persistently infected flies

The *w*^{1118} fly stocks persistently infected with DAV, DCV, or Nora virus have been described previously.[36] The *w*^{1118} fly stock persistently infected with Bloomfield virus was generated as described previously.[36] Briefly, a Dipt-GFP reporter fly stock (BDSC Cat# 55709) was found to be contaminated with Bloomfield virus during routine screening. We homogenized the infected flies in PBS (5 μl/fly) and filtered the homogenate through a 0.22 μm filter. The homogenate was injected into 20 female and 10 male *w*^{1118} flies (50 nl/fly) and the injected flies were placed in fresh vials containing standard cornmeal diet. After 3 days, the injected flies (F0) were removed and the F1 was reared in the same vial. The F1 flies were moved to a fresh vial 5 days after eclosion of the first adults. The F1 flies were removed from this vial after 9 days and F2 flies were moved to a new vial 5 days after eclosion of the first adults. The F2 was treated in the same manner and F3 adults were taken as the persistently infected stock. The presence of Bloomfield virus and the absence of other known *Drosophila*-infecting viruses was confirmed by total RNA sequencing.

METHOD DETAILS

Viral infections

All infections were performed using groups of 20-40 mated adult female flies (3-5 days old). All infections were performed at 29 °C and infected flies were maintained at 29 °C unless otherwise stated. Flies were moved from their rearing temperature to 29 °C 24 hours prior to infection and starved for 5 hours prior to infection. Inoculation of standard cornmeal diet was performed by evenly coating the surface of the fly food with 100 μl of a DAV stock (1.3-2.0 x 10^3 oral infectious dose 50% units/ml, see viral stock preparation and titration details below). Flies were placed on the contaminated food immediately following inoculation and were maintained on the contaminated food for 24 hours before being moved to fresh vials in groups of 20 flies/vial. The time at which flies were moved from the contaminated vials to fresh vials was considered as 0 dpi. Subsequently, the flies were flipped to fresh vials every two days. Mock-infections were performed in the same manner.

For experiments involving persistently-infected flies (as in Figures 2C, S1F, and S1G), 10 males and 10 females of unknown age were collected from standard rearing vials for each persistently-infected stock or from standard rearing vials of uninfected *w*^{1118} flies. These flies (referred to as the F0) were placed in fresh vials at 25 °C. 10 vials were setup in this manner for each fly stock and the F0 flies were removed after 10 days. The F1 flies (males and females together) were collected on the day of eclosion (referred to as 0 days-post eclosion) and moved to 29 °C. After 24 hours, the male F1 flies were removed and the female F1 flies were sorted into fresh vials at a density of 20 flies/vial. Subsequently, the flies were flipped to fresh vials every two days.

Ecc15 infections

Ecc15 infections were performed at 29 °C using groups of 30 mated adult female flies (3-5 days old). Flies were moved from their rearing temperature to 29 °C 24 hours prior to infection and starved for 2 hours prior to infection. Inoculation of 5% sucrose agar vials was performed by placing a piece of Whatman filter paper on the surface of the media and applying 600 μl of infection solution directly to the filter paper. Infection solution consisted of 300 μl of Ecc15 (OD$_{600}$ = 200) in Luria-Bertani broth mixed with 300 μl of 5% sucrose. Mock infection solution consisted of 300 μl of Luria-Bertani broth mixed with 300 μl of 5% sucrose. Flies were fed on the infection solution for 24 hours before midgut dissection.

Antibody production

A polyclonal antibody against the DAV capsid protein (referred to as anti-DAV) was produced by GenScript Biotech (Piscataway, New Jersey, United States) using the PolyExpress Polyclonal Antibody Service. Briefly, New Zealand rabbits were immunized with the entire DAV capsid protein (GenBank accession no. YP_003038596) expressed in and purified from *E. coli* and anti-DAV was purified from the sera of immunized rabbits by affinity purification. The sensitivity and specificity of anti-DAV was verified by ELISA and western blot.

Viral stock preparation and titration

DAV stocks used for all experiments were prepared from w^{1118} flies persistently infected with DAV. Flies of mixed ages and sex were collected from standard rearing vials and homogenized in 1x PBS (3 μl/fly). Homogenates were snap-frozen in a bath of dry ice/70% ethanol, stored overnight at -80 °C, thawed on ice, and clarified twice by centrifugation at 15,000 x g for 10 minutes at 4 °C. The clarified homogenate was filtered through a 0.22 μm filter and single use aliquots (100 μl) were snap-frozen in a bath of dry ice/70% ethanol and stored at -80 °C. A mock viral stock was prepared in the same manner using uninfected w^{1118} flies.

DAV stocks were titered by 50% endpoint dilution via *in vivo* oral infection in adult flies to calculate an oral infectious dose 50% (OID_{50}) for DAV stocks. The presence or absence of infection at 12 dpi was determined by ELISA in individual flies infected with a dilution series of DAV stock to calculate the OID_{50} according to the Reed and Muench method.[86] In detail, oral infections were performed as described above using ten-fold serially diluted DAV stocks ranging from undiluted to 10^{-5}. Mock-infected flies served as a negative control. Individual flies (8 flies/dilution) were collected at 12 dpi and homogenized in 100 μl 1x PBS. 20 μl of each homogenate was mixed with 20 μl of lysis buffer (40 mM HEPES, pH 7.5, 2 mM DTT, 200 μM KCl, 10% glycerol, 0.1% NP-40, 1x cOmplete EDTA-free Protease Inhibitor Cocktail (Roche, 11873580001)) and incubated at room temperature for 15 minutes. 10 μl of the homogenate:lysis buffer mixture was added to 190 μl of 0.05 M carbonate-bicarbonate buffer, pH 9.6 in an Immuno 96-well flat bottom clear non-sterile plate, Nunc, MaxiSorp (Thermo Fisher, 442404) and incubated for 2 hours at room temperature. The plate was then washed three times with 200 μl/well of 1x PBS, 0.05% Tween-20 and incubated at room temperature for 2 hours with 200 μl/well of blocking buffer (1x PBS, 0.05% Tween-20, 5% non-fat dry milk). The plate was then washed three times with 200 μl/well of 1x PBS, 0.05% Tween-20 and incubated overnight at 4 °C with 100 μl/well of anti-DAV diluted 1:2000 in blocking buffer. The plate was then washed four times with 200 μl/well of 1x PBS, 0.05% Tween-20 and incubated at room temperature for 2 hours with 100 μl/well of donkey anti-rabbit IgG-HRP (Cytiva, NA934) diluted 1:2000 in blocking buffer. The plate was then washed four times with 200 μl/well of 1x PBS, 0.05% Tween-20 and incubated at room temperature for 2 hours with 100 μl/well of 1-Step Turbo TMB-ELISA substrate solution (Thermo Fisher, 34022). The reaction was stopped by addition of 100 μl/well of 2N HCl and absorbance at 450 nm was read on a Tecan Infinite M200 PRO plate reader. Infection status was determined for each fly based on A_{450} values and the threshold for infection was set as the average A_{450} for mock-infected flies plus ten times the standard deviation of A_{450} for the mock-infected flies. The OID_{50} of DAV stocks was calculated based on the infection prevalence for each dilution according to the Reed and Muench method.[86]

RNA extraction and RT-qPCR

Total RNA was extracted from whole flies, dissected midguts, or carcasses using TRIzol Reagent (Invitrogen, 15596026) according to the manufacturer's instructions and RNA concentration was measured with the Qubit RNA BR Assay Kit (Invitrogen, Q10211). Midgut samples were prepared by first dissecting the entire alimentary canal and then carefully removing non-midgut tissues (the Malpighian tubules, the foregut and crop, and all tissues, posterior to the midgut/hindgut junction). Carcasses included the entire fly body with the exception of the head and the alimentary canal.

DAV negative strand-specific RT-qPCR was performed as previously described.[36] Briefly RNA was reverse transcribed with DAV_tag_F (5' AATTCAAGCTCGTCTTCCTCGGTTGGATCAGGCTAGTGTAGG) using SuperScript II Reverse Transcriptase (Invitrogen, 18064022) according to the manufacturer's instructions with the following modifications: reverse transcription was performed at 50 °C for 30 minutes and reactions were heat inactivated for 15 minutes at 95 °C. cDNA was diluted 1:10 with distilled water and qPCR was performed in triplicate 10 μl reactions with the primers Tag_qPCR_F (5' AATTCAAGCTCGTCTTCCTCG) and DAV_qPCR_R (5' TGCAACCGGACTCCAAGTTC) using Luminaris Color HiGreen qPCR Master Mix, low ROX according to the manufacturer's instructions (Thermo Scientific, K0374). qCPR was performed with a QuantStudio 7 Flex instrument (Applied Biosystems). The starting quantity of negative strand DAV RNA in each reverse transcription reaction was determined by absolute quantification by comparison to a standard curve generated by RT-qPCR of ten-fold serially diluted negative strand DAV RNA ranging from 10^2 to 10^8 copies/reaction. Samples below the limit of detection (10^3 copies/reaction) were considered to have 0 negative strand copies. The number of negative strand copies per tissue was calculated from these data based on the RNA yield for each sample.

To calculate relative DAV RNA levels, RNA was treated DNase I recombinant, RNase-free (Roche, 04716728001) and reverse transcribed with Maxima H Minus First Strand cDNA Synthesis Kit (Thermo Scientific, K1652) according to the manufacturers' instructions. The cDNA was diluted 1:10 with distilled water and amplified in triplicate 10 μl qPCR reactions for each sample and target using Luminaris Color HiGreen qPCR Master Mix, low ROX (Thermo Scientific, K0374) according to the manufacturer's instructions (Thermo Scientific, K0374). DAV RNA was detected with the primers DAV_qPCR_F (5' GTTGGATCAGGCTAGTGTAGG) and DAV_qPCR_R (5' TGCAACCGGACTCCAAGTTC) and Rpl32 RNA was detected with the primers Rpl32_qPCR_F (5' CGGATCGATATGCTAAGCTGT) and Rpl32_qPCR_R (5' GCGCTTGTTCGATCCGTA). Relative DAV RNA levels were determined using the delta-delta Ct method.[87] DAV RNA levels in each sample were normalized to those of Rpl32 and are shown relative to the samples indicated in each figure legend. Relative levels of *stat92e* RNA were measured in the same manner using the primers Stat92e_qPCR_F (5' TAAACTCCACATCCTCGCCG) and Stat92e_qPCR_R (5' GCCAGTTCTTGAGCTCGTGT)

Survival analysis

Survival analyses following oral infection were conducted using biological replicates of 10-20 flies/replicate sorted at 1 dpi. Survival analyses for persistently infected flies were conducted by collecting male and female flies together on the day of eclosion. These flies were allowed to mate for 24 hours before being sorted into replicates of 20 flies/replicate. Survival analyses for persistently infected

flies were done using flies maintained at 25 °C. All statistical comparisons involved flies maintained at identical initial population densities. Survival was monitored daily by counting the number of dead flies in each vial and flies were flipped to fresh vials every two days. For direct comparisons of survival curves (as in Figures 1B, 2C, 3C, S1A, S5D, and S6C), the survival data from all replicates of a given treatment and genotype were pooled and compared using a log-rank (Mantel-Cox) test. As expected, genotype and rearing condition (GF vs. CR) strongly influenced survival even under mock-infected conditions, confounding direct comparison of survival curves for DAV-infected flies of different genotypes or rearing conditions. Thus, we used the relative median survival to compare the influence of DAV infection on survival between different genotypes or rearing conditions while taking into account the different background survival rates of mock-infected flies (as in Figures 3B, 6F–6H, S1C, and S4I). To calculate relative median survival, we first averaged the median survival (in days) of mock- or DAV-infected flies across biological replicates for a given genotype or treatment. We then calculated relative median survival as the average median survival across replicates of DAV-infected flies divided by the average median survival across replicates of mock-infected flies. For example, a relative median survival of 0.6 indicates that the average median survival of DAV-infected flies across biological replicates was 0.6 times that of mock-infected flies. The relative standard deviations of relative median survival values were calculated by propagation of error using the formula:

$$\sigma RMS \,=\, RMS \times \sqrt{\left(\frac{\sigma DAV}{\overline{DAV}}\right)^2 + \left(\frac{\sigma Mock}{\overline{Mock}}\right)^2}$$

Where σRMS = standard deviation of the relative median survival, RMS = relative median survival, σDAV = standard deviation of the median survival for DAV-infected biological replicates, $\overline{DAV}$ = average median survival of the DAV-infected biological replicates, $\sigma Mock$ = standard deviation of the median survival for mock-infected biological replicates, and $\overline{Mock}$ = average median survival of the mock-infected biological replicates. The values of σRMS, RMS, and sample size were used to determine the statistical significance of differences between relative median survival values using a two-tailed T-test.

Smurf assay

Smurf assays for measurement of intestinal barrier function were setup using biological replicates of 20 female w^{1118} flies as described for survival analysis. Beginning from 7 dpi, flies were continuously maintained in vials in which 100 µl of a sterile solution of 32% FD&C blue dye #1 had been evenly spread on the surface of the diet. Following application of the blue dye solution, the vials were left to dry overnight at 25 °C before being used to house flies. Flies were flipped to fresh blue-dye treated vials every two days and "smurfness" was scored daily by examination of flies under a dissection microscope according to Martins et al.[88] Dead flies were thoroughly washed with water to ensure that assessments of their blue coloration were based on internal blue dye rather than blue dye accumulated on external body surfaces. We calculated the median time (in days) until development of the smurf phenotype for each biological replicate and we evaluated the significance of differences in these median values between replicates of mock- and DAV-infected flies using a two-tailed T-test.

RNA FISH, immunofluorescence, and imaging

For detection of positive strand DAV RNA by RNA FISH, whole digestive tracts were dissected from mock- or DAV-infected flies in 1x PBS over a period of 20 minutes. Dissected tissues were subsequently fixed in 4% paraformaldehyde, 0.3% Tween-20 for 20 minutes, washed twice for 2 minutes each time with 1x PBT (1x PBS, 0.1% Triton X-100), and then permeabilized by incubation in 1x PBS, 0.5% Triton X-100 for 20 minutes. Permeabilized tissue samples were washed for 2 minutes and then again for 10 minutes in fresh wash buffer (10% deionized formamide, 2x SSC) at room temperature. Finally, tissue samples were washed again with prewarmed wash buffer at 37 °C for 5 minutes and then incubated overnight with gentle shaking at 37 °C in prewarmed hybridization buffer containing 200 nM of 3′ ATTO 647-labeled DAV-specific oligonucleotides synthesized by DNA Script using a SYNTAX STX-200 instrument[89] (see Table S1 for oligonucleotide sequences, all oligonucleotides were mixed in equimolar amount). The hybridization buffer consisted of 10% deionized formamide, 5% dextran sulfate, 2x SSC, and 200 nM labeled oligonucleotides. The next day, tissue samples were washed for 2 minutes in fresh washer buffer and then rinsed three times for 10 minutes each time in 2x SSC. Subsequently, tissue samples were washed in 1x PBT for 2 minutes and then again for 10 minutes. DAPI was added to the second PBT wash at a final concentration of 1 µg/ml. Finally, tissue samples were mounted in 4% N-propyl-gallate, 80% glycerol.

For immunofluorescence of digestive tissues, whole digestive tracts were dissected in 1x PBS over a period of 20 minutes and placed directly into 4% paraformaldehyde for fixation. Fixation continued for an additional 50 minutes following the end of the 20 minute dissection period. Fixed tissues were washed for 10 minutes three times (30 minutes total) in 1x PBT, incubated in 1x PBS, 50% glycerol for 30 minutes, and then equilibrated in 1x PBT for 30 minutes prior to incubation with primary antibodies diluted in 1x PBT. Primary antibody incubation occurred overnight at 4 °C. Tissues were then washed for 10 minutes three times before incubation with secondary antibodies diluted in 1x PBT. Secondary antibody incubation occurred for 3-5 hours at room temperature. Finally, tissues were washed for 10 minutes three times (the final wash contained 1 µg/ml DAPI) and mounted in 4% N-propyl-gallate, 80% glycerol. The following primary antibodies were used: anti-DAV (rabbit, 1:1000, generated in this study), anti-Delta (mouse, 1:1000, DSHB, c594.9b), anti-Prospero (mouse, 1:1000, DSHB, MR1A), anti-PH3 (rabbit, 1:1000, Merck Millipore, 06-570), anti-GFP (chicken, 1:2000, Invitrogen, A10262). Anti-Delta (DSHB, c594.9b) and anti-Prospero (DSHB, MR1A), developed by Artavanis-Tsakonas, S and Doe, C.Q., respectively, were obtained from the Developmental Studies Hybridoma Bank, created by the NICHD of the NIH and maintained at The University of Iowa, Department of Biology, Iowa City, IA 52242. The following secondary antibodies were

used: anti-rabbit 647 (goat, 1:500, Invitrogen, A-21244), anti-mouse-488 (goat, 1:500, Invitrogen, A-11029), anti-chicken-488 (goat, 1:500, Invitrogen, A32931). All imaging was performed on a Zeiss LSM 700 confocal microscope at the Institut Pasteur Unit of Technology and Service Photonic Bioimaging platform. All images are single Z-slices. For experiments involving comparison of one or more images, images within the experiment were acquired using the same settings and any post-acquisition modifications were applied equally to images of control and experimental samples.

RNA-seq analysis

For the RNA-seq data depicted in Figures 4 and S3, CR or GF flies were infected as described above. Midguts were dissected at 6 and 12 dpi in 1x PBS. Midguts were dissected in 5 pools of 5 guts/pool, placed in 40 μl of ice-cold 1x PBS, and immediately transferred to dry ice upon dissection of each pool. Midgut samples included only the midgut portion of the alimentary canal as described for RNA extraction above. RNA was extracted from midgut pools using 300 μl TRIzol reagent according to the manufacturer's instructions. RNA-seq libraries were prepared with 150 ng RNA from 4 randomly selected pools/condition using a TruSeq Stranded mRNA Library Prep kit (Illumina, 20020595) with IDT for Illumina TruSeq RNA UD Indexes (Illumina, 20022371).

For the RNA-seq data depicted in Figures 7 and S7, flies were infected as described above. Midguts were dissected at 8 dpi. Individual midguts (12 midguts/condition) were dissected in 1x PBS, immediately transferred to 40 μl of ice-cold 1x PBS, and placed on dry-ice. RNA was extracted from individual midguts using 300 μl TRIzol reagent according to the manufacturer's instructions. RNA concentrations were measured using the Qubit RNA BR Assay Kit (Invitrogen, Q10211). Within each condition, individual midguts were randomly assigned to 4 pools of 3 midguts/pool and 50 ng RNA from each individual midgut was combined to prepare the RNA pools. RNA-seq libraries were prepared from 150 ng of pooled RNA using an NEBNext Ultra II RNA Library Prep Kit for Illumina (New England Biolabs, E7770L) with NEBNext Multiplex Oligos for Illumina (Dual Index Primers Set 1) (New England Biolabs, E7600S). All sequencing was performed on an Illumina NextSeq 500 instrument using a NextSeq 500/550 High Output Kit v2.5 (75 cycles)(Illumina, 20024906).

Reads were mapped to the *D. melanogaster* genome (release dmel_r6.43) with STAR[81] (version 020201). Feature counting was performed with HTSeq[82] (version 0.6.1p1) using the default settings and differential gene expression analysis was performed with DESeq2[64] in R Studio (version 2023.03.1)[83]. Log$_2$ fold changes were shrunken using the ashr algorithm and only adjusted p-values were considered for analysis.

Gene Ontology enrichment analysis

Gene Ontology enrichment analysis was performed with the g:GOSt function of g:Profiler[63] using the default settings.

QUANTIFICATION AND STATISTICAL ANALYSIS

All plots of data were prepared using ggplot2 in R Studio (version 2023.03.1)[83]. Confocal images were minimally processed in ImageJ (version 1.53t). Adjustments made to raw images included cropping, annotation, and adjustments to brightness and contrast applied across the entire image. Figures were assembled in Inkscape (version 0.92). Statistical analyses were performed using the GraphPad Prism software (version 9.5.1). Mitotic cells (PH3+ cells) were counted manually in the entire midgut and analyzed using Kruskall-Wallis tests or by two-way ANOVA with Turkey's post-hoc tests. For scoring of Esg+ cells, total nuclei and Esg+ nuclei were identified using QuPath[84] (version 0.4.3) in unprocessed confocal images acquired at 25x from R2 and R4 midgut regions. Analysis regions were defined manually for each image to include the entire region of the midgut present in the field, but to exclude non-target tissues that were occasionally present in the field (Malpighian tubules, non-target midgut regions present due to the orientation of the mounted tissue sample, and other midguts located nearby on the slide). Proportions of Esg+ cells were analyzed by two-way ANOVA with Turkey's post-hoc tests. Survival was analyzed by log-rank (Mantel-Cox) tests and two-tailed T-tests as described under survival analysis. Adjusted p-values associated with RNA-seq data are the results of Wald tests as implemented in DEseq2.[64] Negative-strand DAV RNA levels and relative DAV RNA levels obtained by RT-qPCR were analyzed using two-tailed T-tests. Complete details regarding the statistical tests used, sample sizes, dispersion and precision measures, and definitions of significance are reported in the figure legends.